Tephrochronology of the central Mediterranean MIS 11c interglacial (~425-395 ka): new constraints from the Vico volcano and Tiber delta, Central Italy

Alison Pereira[1,2,3], Lorenzo Monaco[4], Fabrizio Marra[5], Sébastien Nomade[3], Mario Gaeta[4], Niklas Leicher[6], Danilo M. Palladino[4], Gianluca Sottili[4], Hervé Guillou[3]; Vincent Scao[3], Biagio Giaccio[7]

1 Ecole française de Rome, Piazza Farnese, IT-00186, Roma, Italy

2 Département Hommes et environnements, Muséum national d'Histoire naturelle, UMR 7194 du CNRS, 1 rue René Panhard, 75013 Paris, France.

3 Laboratoire des Sciences du Climat et de l'Environnement, LSCE/IPSL, CEA-CNRS-UVSQ, Université Paris-Saclay, F-91191 Gif-sur-Yvette, France.

4 Sapienza Università di Roma, Dipartimento di Scienze della Terra, Piazzale Aldo Moro 5, 00185 Roma, Italy

5 Istituto Nazionale di Geofisica e Vulcanologia, Rome, Italy

6 Germany Institute of Geology and Mineralogy, University of Cologne, Cologne, Germany

7 Istituto di Geologia Ambientale e Geoingegneria, CNR, Roma, Italy

Keywords

Tephrochronology; $^{40}Ar/^{39}Ar$, MIS 11c interglacial; Central Mediterranean; Vico volcano.

Abstract

Through a systematic integrated approach, which combined lithostratigraphic, geochronological and geochemical analyses of tephra from near-source sections of the peri-Tyrrhenian volcanoes and mid to distal settings, here we provide an improved tephrochronological framework for the Marine Isotope Stage 11c interglacial (MIS 11c, ~425-395 ka) in the Central Mediterranean area. Specifically, we present the complete geochemical dataset and new high-precision $^{40}Ar/^{39}Ar$ ages of the previously poorly characterized earliest pyroclastic products of the Vico volcano (420-400 ka), including the Plinian eruptions of Vico α and Vico β and the immediately post-dating lower magnitude explosive events. Furthermore, we also provide new geochronological and geochemical data for the distal tephra layers preserved in the aggradational succession of the Tiber delta (San Paolo Formation), Roman area, which records sea level rise relating to the MIS 12 (glacial) to MIS 11 (interglacial) transition. Five pyroclastic units were recognised in Vico volcanic area, four out of which, Vico α, Vico β, Vico β_{top} (a minor eruption immediately following Vico β and temporally very close to it) and Vico δ were directly dated at 414.8 ± 2.2 ka, 406.5 ± 2.4 ka, 406.4 ± 2.0 ka and 399.7± 3.2 ka respectively (2σ analytical uncertainties). These new data allow a critical reappraisal of the previously claimed identifications of Vico tephra from mid-distal to ultra-distal successions (i.e., Vico-Sabatini volcanic districts, Roman San

Paolo Formation and Castel di Guido archaeological site, Sulmona Basin, Valdarno and Lake Ohrid), which were unavoidably biased by the poor and incomplete geochemical and geochronological reference datasets previously available. Such an improvement of the tephrochronological framework brings great benefits to any future investigations (e.g., paleoclimatology, archaeology, active tectonic, volcanology) in the dispersal areas of the studied eruptions at the key point in time that is MIS 11.

1. INTRODUCTION

High-precision chronologies and reliable correlations of sedimentary records are essential requirements to reconstruct and understand the Earth's system evolution. However, despite the continuous efforts to improve the geochronological methods (e.g., Kuiper et al., 2008; Reimer et al., 2013), establishing robust chronologies beyond ~50 ka, i.e., the radiocarbon limit, remains a challenging task. This is particularly true in continental setting, where astrochronology, commonly used for dating marine records, is less applicable. Among other geochronometers, tephrochronology is recently arising as an outstanding dating-correlation tool for addressing with a robust chronological control several Quaternary sciences issues (e.g., Lowe et al., 2011). Through radioisotope dating and geochemical fingerprinting of tephra layers interbedded within sedimentary archives, tephrochronology allows the correlation of palaeoenvironmental records and their integration in a coherent chronological framework, independent of orbital tuning approaches (e.g., Giaccio et al., 2015; Mannella et al., 2017; 2019; Regattieri et al., 2014; Wulf et al., 2018; Zanchetta et al., 2011; 2016). Equally significant are the applications of the distal tephrostratigraphy for volcanological purposes, which, through the integration of the data collected in near-source areas, allows to improve the knowledge of the eruptive history and dynamics of adjoining volcanoes (e.g., Paterne et al., 2008; Costa et al., 2012; Insinga et al. 2014; Petrosino et al., 2014; Bourne et al., 2015; Albert et al., 2019; Wulf et al., 2012; 2020).

The present work deals with the first part of the Marine Isotope Stage 11 (MIS 11), roughly corresponding to the MIS 11c interglacial period (c.a. 425 ka to 395 ka) in western Mediterranean. Among Middle Pleistocene interglacial phases, MIS 11c is of great interest as, along with the MIS 19c interglacial, it is considered as one of the closest analogues of the Holocene orbital configuration, mainly for the low eccentricity conformity of these periods (Berger et Loutre, 2003, Healey and Thunell, 2004). This interglacial occurred during a phase of relatively weak insolation forcing (spanning two insolation peaks) and took place after the MIS 12 period (478-430 ka) that stands out as one of the most arid, coldest and longest glacial periods of the Quaternary (Shackleton, 1987, Tzedakis et al., 2003, Masson-Delmotte et al., 2010, Rohling et al., 2014). On the contrary, the MIS 11c interglacial is probably one of the warmest and longest (20-30 kyrs) Quaternary interglacials (Karner and Marra, 2003), making the MIS 12-MIS 11 transition by far the most contrasting deglaciation with the highest amplitude over the past 5 Ma (Bowen, 2009, Dutton et al., 2015).

Our study focuses on the central area of the Italian peninsula, which is a privileged region for Middle Pleistocene tephrochronological, paleoclimatic and paleoenvironmental studies. The peculiar geodynamic context of the Mediterranean, characterized by both intense tectonic and volcanic activities, often fed by ultrapotassic magma, makes this region suitable for the development of continental tectonic basins hosting long and continuous sedimentary successions which are ideally suited to providing rich tephra records (e.g., Karner and Renne, 1998; Karner and Marra, 1998; Marra et al., 1998, 2008, 2016; Amato et al. 2018; Giaccio et al., 2013, 2015, 2017, 2019; Petrosino et al. 2014; Leicher et al., 2019). This unique situation allows for the anchoring of multi-proxy and archaeological records to robust chronologies, which are acquired thanks to both direct (i.e., via high-precision and accurate $^{40}Ar/^{39}Ar$ dating of K-rich crystals) and indirect (i.e., via geochemical fingerprinting) dating approaches (e.g., Marra et al., 2008; 2016, 2015, 2017a, 2017b; Giaccio et al., 2015, Regattieri et al., 2014, 2016, 2017, 2019; Sagnotti et al., 2014, Mannella et al., 2019, Pereira et al., 2015, Peretto et al., 2015, Villa et al., 2016, Pereira et al., 2018).

However, despite recent progress, the potential of the central Mediterranean Middle Pleistocene tephrochronology is still under-exploited due to the lack of geochronological and geochemical reference datasets for both near-source and distal tephra archives (e.g., marine/lacustrine sedimentary successions). To unlock the full potential of tephrochronology during this interval we provide a comprehensive major element volcanic glass geochemistry and geochronological dataset for the early explosive activity of Vico Volcano (Period I, Perini et al., 2004), including the Plinian eruptions of Vico α and Vico β. This volcanic activity has been framed so far in the interval 425-403 ka (Barberi et al., 1994; Marra et al., 2014b) and is therefore potentially crucial to constraining the chronologies of MIS 11c regional sedimentary records. Mid-distal equivalent deposits of the Vico activity have been tentatively identified within the aggradational successions of the Paleo-Tiber River, which are key sedimentary archives for independently constraining the chronology of the sea-level rise during the glacial terminations (Marra et al., 2016, and references therein). Furthermore, tephra related to the early Vico activity have been tentatively also recognized in distal and ultra-distal sedimentary archives, such as Valdarno, central Italy (Marcolini et al., 2003), Sulmona Basin, central Italy (Regattieri et al., 2014) and Lake Ohrid, Macedonia-Albania (Kousis et al., 2018). However, up to now, the proposed identification of the Vico main tephra has been based on an analytically inadequate geochemical dataset and/or imprecise geochronological constraints, making these early recognitions quite uncertain and poorly supported. The new stratigraphical, geochronological and geochemical data presented in this paper provide an improved regional to extra-regional tephrochronological framework for the central Mediterranean MIS 11c interglacial interval. Specifically, these new datasets allow us to refine the chronology of the Roman archaeological-paleontological sites (e.g., Marra et al., 2018) and of paleoclimatic-environmental changes recorded within Mediterranean sedimentary archives (e.g., Lake Ohrid, Sadori et al., 2016, Wagner et al., 2017, 2019, Kousis et al., 2018; Sulmona Basin, Regattieri et al., 2014). Furthermore, the same data bring new insights on the timing and dynamic of the sea-level variations during the late MIS 12-early MIS 11 (Marra et al., 2016), which we are going to address elsewhere (Giaccio et al., in preparation).

2. PREVIOUS INVESTIGATIONS

2.1. The Vico volcano explosive activity (~420-93 ka)

The Vico is a central caldera-volcano with a small number of post-caldera monogenetic centres developed within the NW–SE Siena-Radicofani and Paglia-Tevere extensional basin (Barberi et al., 1994). It is located in the northern part of the Roman comagmatic province (South of the Vulsini volcanic District) and partially overlies the Cimini volcanoes (see Fig. 1) that were active during the Lower Pleistocene (1.3-0.9 Ma) (Locardi et al., 1977). Eruptive activity at Vico is loosely constrained between ~420 to ~95 ka. Three main periods of eruptive activity were recognized for this volcanic centre: (i) the Vico Period I (~ 420-400 ka), mainly composed of latite, trachyte, and rhyolite pyroclastic fall deposits and minor lava flows; (ii) the Vico Period II (~ 305 to 138 ka), dominated by intermediate to felsic leucite-bearing lavas; (iii) the Vico Period III (~ 138 to 95 ka), corresponding to the post-caldera activity, was associated to both leucite-free and leucite-bearing mafic lavas, scoria fall, and phreatomagmatic products (Cioni et al., 1987; Laurenzi and Villa, 1987; Perini et al., 2004). This study is focused on the Vico Period I (or Rio Ferriera Formation; Perini et al., 2004) which was characterized by Plinian to sub-Plinian eruptions as evidenced by widely dispersed and thick pyroclastic fall deposits. The two main explosive events of this eruptive period were firstly described by Cioni et al. (1987) and labelled Vico α and Vico β. Deposits of Vico α are mostly found in the northern part of the edifice, from Viterbo to Vignanello-Orte, while Vico β, that is stratigraphically above Vico α, and is mainly dispersed in the eastern sector of the volcano (Fig. 1a; Cioni et al., 1987). Whole rock composition of the Vico Period I, reveals a wide geochemical variability, ranging from latites to trachytes and rhyolites (Cioni et al., 1987; Perini et al., 2004). The currently available age determination for both Vico α and Vico β units are 419.0 $\pm$ 6.0 ka (Laurenzi and Villa, 1987) and 403.0 $\pm$ 6.0 ka (Barberi et al., 1994) (uncertainties at 2σ).

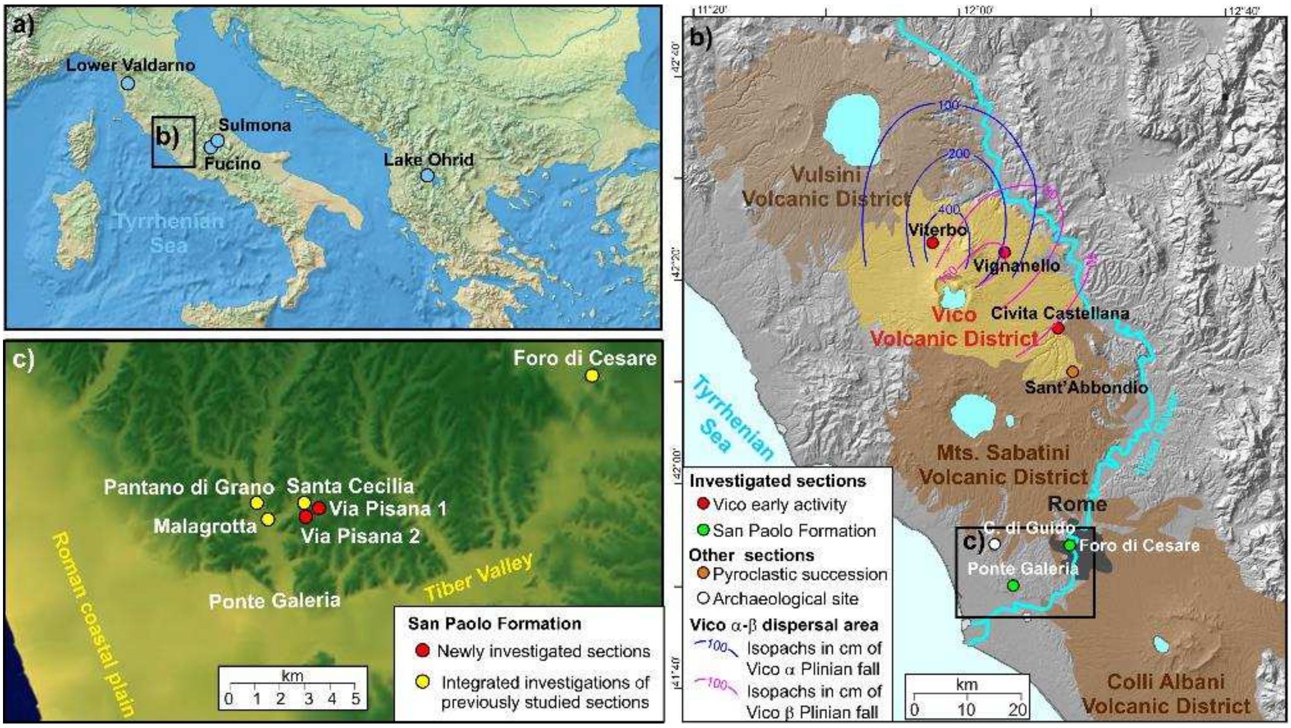

Figure 1. Reference maps. **a)** Geographic setting of the Latium volcanic districts including the investigated sections, showed in panel b, and location of other records cited in the text (blue circles). **b)** Geological sketch map of the Latium volcanic districts (Roman Province), showing the locations of the investigated sections and the isopachs of the Vico α and Vico β Plinian deposits (from Cioni et al., 1987). **c)** Detailed map showing the locations of the San Paolo Formation investigated sections.

2.2. Tiber River terraces: San Paolo aggradational succession (MIS 11)

The study of the San Paolo Formation (SPF through the text) sedimentary succession has been continuously carried out and improved since the 90's (Fig. 2). This succession has been proved to record the MIS 12 deglaciation and the MIS 11 high-stand in the Roman coastal area, allowing to independently constrain the age of the glacio-eustatic sea level rising (Karner and Renne, 1998; Karner et al., 2001; Marra et al., 2016; 2017a).

Within the aggradational succession of the San Paolo Formation four sub-primary pyroclastic layers were identified, with some $^{40}Ar/^{39}Ar$ dated (see Fig. 2). For consistency, all the $^{40}Ar/^{39}Ar$ ages presented in this study are given at 2σ analytical uncertainties and when possible were recalculated according to the K total decay constant of Renne et al., 2011 and the flux standard ACs-2 dated to 1.1891 Ma (Niespolo et al., 2017). While the topmost volcaniclastic layer SPF4 (Fig. 2) has never been dated, the uppermost available chronological limit of the SPF was provided by the $^{40}Ar/^{39}Ar$ age of the sub-primary pumice fallout SPF3 at 413.5 ± 2 ka (2σ uncertainties, recalculated from Karner et al., 2001), labelled Ponte Galeria Bedded-Pumice in Karner et al. (2001) and C7 in Marra et al. (2016) (Fig. 2).

The lowermost chronological limit for the late MIS 12-MIS 11 SPF is instead provided by two $^{40}Ar/^{39}Ar$ analyses of the layer SPF1, which provided a combined age of 435.6 ± 6.1 ka (sample R95-04H+PdG-S2, 2σ uncertainties, Marra et al., 2016, Fig. 2).

An age of the middle part of the San Paolo Formation was obtained. At Malagrotta waste refusal site, the $^{40}Ar/^{39}Ar$ dating of a primary ash-fall layer at higher elevation with respect to the layer SPF1 of Pantano di Grano (Fig. 2), yielded the age of 423.5 ± 5 ka (2σ uncertainties) for these deep lagoon sediments (sample R94-30C in Karner and Renne, 1998). A further age of 419.5 ± 6 ka (2σ uncertainties) was determined for a white pumice layer occurring in a fluvial-alluvial plain succession outcropping in the archaeological area of the Foro di Cesare (sample FC-SP-01, Capitoline Hill, Rome in Marra et al., 2016) (Figs. 1b and 2). This sedimentary succession occurs at only 15 m a.s.l., i.e. largely below the average elevation of the undisturbed deposits of the SPF, possibly due to a local tectonic lowering (Fig. 2). Considering its age and whole rock-glass geochemical composition, this white pumice fall was tentatively correlated either to SPF2 (R94-30C) cropping out at Malagrotta (Marra et al., 2016), or to Vico α Plinian eruption (Marra et al., 2014b).

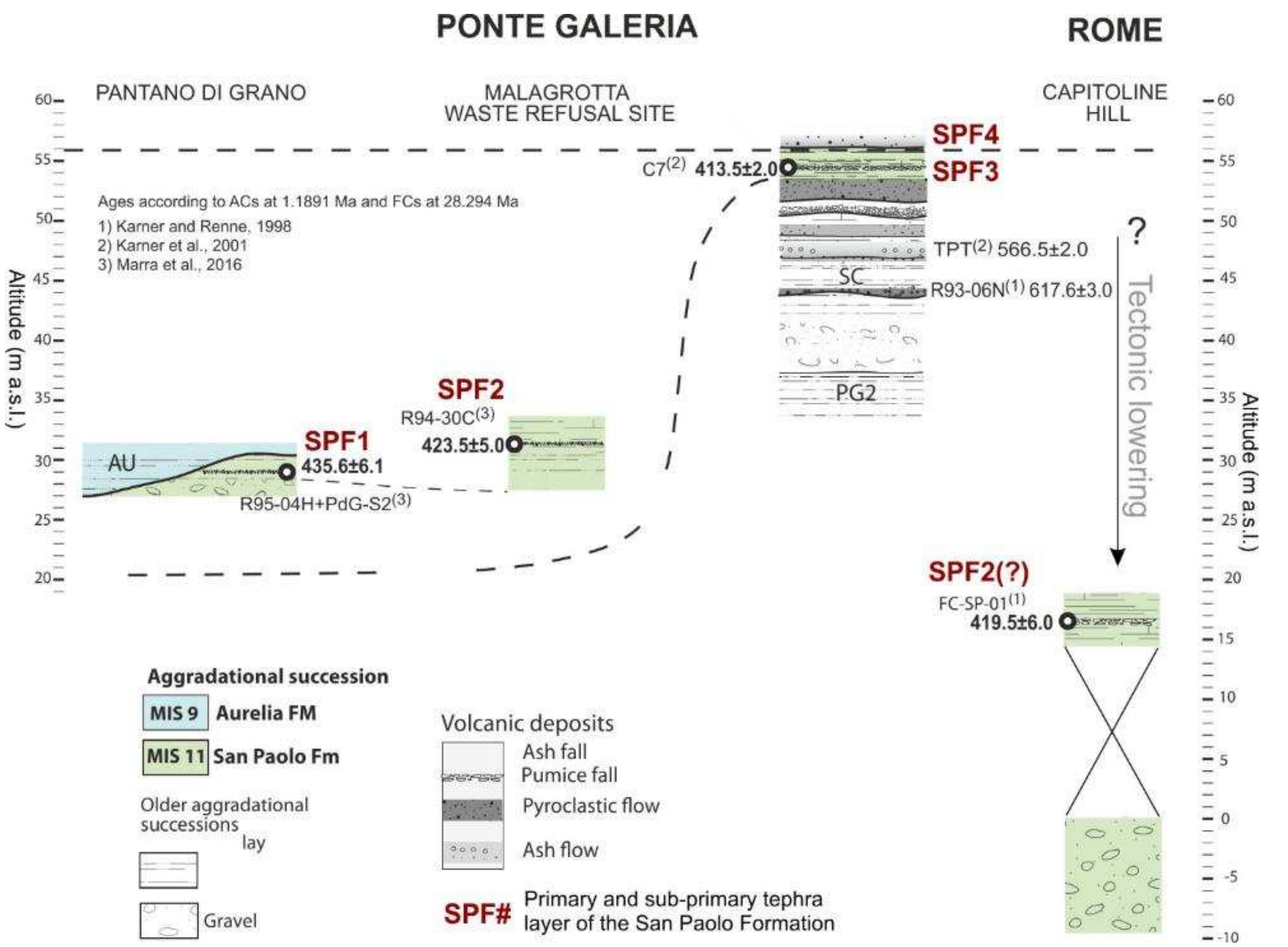

Figure 2. Stratigraphic logs summarizing the sedimentary settings and chronological constraints available for the MIS 12-MIS 11 aggradational succession of the San Paolo Formation (modified from Marra et al. 2016). Ages are reported at 2σ analytical uncertainties. In Karner and Renne, (1998) it is not specifically indicated which standard (ACs, FCs or BTs) has been co-irradiated with the individual samples. By default, we have recalculated their ages presuming they were initially dated according to ACs.

3. MATERIALS AND METHODS

3.1. Field investigations and sampling

3.1.1. Vico volcano area

Three sections have been investigated in the Vico volcanic area (Tab. 1; Fig. 1) and have been stratigraphically and lithologically characterized by direct field observations and lithofacies analyses. Two proximal sections documenting the earliest activity of the Vico volcano (Vico Period I of Perini et al., 2004) have been sampled at Viterbo and Vignanello, representing the type localities of the Vico α and Vico β eruptive successions, respectively, as described by Cioni et al. (1987) (Figs. 1 and 3). A third, relatively proximal section was investigated at Civita Castellana, located within the dispersal area of the Vico β Plinian fall (Figs. 1 and 3).

Table 1. Locations of the studied sections and indications of the new investigations carried out in this study. [1]Marra et al. (2020), [2] Karner et al., (2001), [3]Karner and Renne, (1998), [4]Marra et al., (2016), [5]Marra et al., (2014b).

Geological setting	Site/Section	Unit ($^{40}Ar/^{39}Ar$ *sample*)	New investigations: Stratigraphy	New investigations: $^{40}Ar/^{39}Ar$ dating	New investigations: WDS glass-composition	Latitude and longitude
Earliest Vico pyroclastic successions- Proximal sections from Vico	Viterbo	Vico α (*VT-1A*)	Yes	Yes	Yes	42° 23' 82.90" N 12° 17' 60.50" E
		Pre-Vico α	Yes	No	Yes	
	Vignanello	Vico δ (*Vig-6*)	Yes	Yes	Yes	
		Vico β_{top} (*Vig-4*)	Yes	Yes	Yes	
		Vico β (*Vig-1Top*)	Yes	Yes	Yes	
		Base Vico α	Yes	No	Yes	
		Pre-Vico α	Yes	No	Yes	
Mid-distal Vico succession	Civita Castellana	Vico δ	Yes	No	Yes	42° 16' 43.85" N 12° 24' 42.00" E
		Vico γ	Yes	No	Yes	
		Vico β_{top}	Yes	No	Yes	
		Vico β	Yes	No	Yes	
		Inter-Vico α-β	Yes	No	Yes	
		Vico α (*CC1*)	Yes	Yes	Yes	
		Pre-Vico α	Yes	No	Yes	
Rome MIS 11 aggradational succession (San Paolo Formation)	Via della Pisana 1	SPF4 (*P1-C8*)	Yes	Yes	Yes	41° 50' 53.00" N 12° 21' 49.00" E
		SPF3a (*P1-C7*)	Yes	Yes	No	
		SPF3 (*P1-C5*)	Yes	No	No	
	Via della Pisana 2	SPF4 (P2-C1)	Yes	No	Yes	41° 50' 30.00" N 12° 21' 13.00" E
		SPF3a (P2-C2)	Yes	No	Yes	
		SPF3 (P2-C3)	Yes	Yes	Yes	
	Santa Cecilia	SPF4 (*SC-11*)	Yes	Yes	Yes	41° 50' 43.62" N 12° 21' 11.60" E
		SPF3a (*SC-10b*)	Yes	Yes	No	
		SPF3 (SC-10 =C7)	Yes	No (413.5 ± 2 ka[2])	No	
	Malagrotta	SPF2 (R94-30C)	Yes - archive documents	No (423.5 ± 5 ka[3])	Yes	41° 50' 51.00" N 12° 20' 00.00" E
	Pantano Di Grano	SPF1 (PdG-S2/R95-04H)	Yes - archive documents	No (436.5 ± 6 ka[4])	No	41° 51' 26.00" N 12° 19' 40.00" E
	Foro Di Cesare	SPF2 (SPFM)	No	No (419.5 ± 6 ka[5])	Yes	41° 50' 54.00" N 12° 19' 59.00" E
Ultra-distal	Lake Ohrid	OH-DP-1733	No	No	Yes	41°02'57.00'' N 20°42'54.00'' E

3.1.2. MIS 12-11 aggradational succession of the San Paolo Formation

Three homologue fluvial-deltaic successions outcropping in the Ponte Galeria area were investigated here. These include the previously investigated and above described Santa Cecilia section (Fig. 2) and two newly discovered sections at Via della Pisana (sections Pisana 1 and 2), located very close to the Santa Cecilia section (Fig. 1b). Here, we identified a previously unrecognized volcanoclastic layer in-between SPF3 and SPF4 labelled SPF3a (Fig. 4).

Table 2. List of the samples analysed for glass major element composition (EMPA-WDS analysis). See Figure 1 and Table 1 for the section locations.

Geological Setting	Section	Tephra unit	Sample Label	Rock-Type
Earliest Vico pyroclastic successions - Proximal sections from Vico	Viterbo	Vico α – Upper Fall	VT-1A VT-1B VT-1C	
		Vico α – Ash Flow	VT-0	
		Vico α – Lower Fall	VT base Vα	
		Pre-Vico α	VT-S	Phonolite
	Vignanello	Vico δ (VIG-E)	Vig-6	Phonolite-Trachyte
		Vico γ (VIG-D)	Vig-5	Trachyte
		Vico β_{top} (VIG-C2)	Vig-4	Phonolite-Trachyte
		Vico β (VIG-C1)	Vig-1b Vig-1t Vig-2 Vig-3	Rhyolite-Trachyte
		Vico α Lower Fall (VIG-B)	Vig-F4 Vig-F3 Vig-F2	Trachyte-Rhyolite
		Pre-Vico α (VIG-A)	Vig-F1 Vig-F1B	Phonolite
Mid-distal Vico succession	Civita Castellana	Vico δ (CC-5)	CC-5	Phonolite-Trachyte
		Vico γ (CC-4)	CC-4	Trachyte-Rhyolite

		Vico β_{top} (CC-3b)	CC-3b	Trachyte-Rhyolite
		Sabatini unknown (CC-2)	CC-2b CC-2a	Phonolite
		Vico α (CC-1)	CC-1b CC-1a	Trachyte Rhyolite
		Vico β (CC-3a)	CC-3a	Rhyolite-Trachyte
		Pre-Vico α (CC-0)	CC-0	Phonolite
Rome MIS 11 aggradational succession (San Paolo Formation)	**Via della Pisana 2**	SPF4	P2-C1	Rhyolite
		SPF3a	P2-C2	Rhyolite-Trachyte
		SPF3	P2-C3	Rhyolite
	Santa Cecilia	SPF4	SC-11	Foidite-Rhyolite
	Via della Pisana 1	SPF4	P1-C8	Foidite
	Foro di Cesare	SPF3	SPFM	Trachyte-Rhyolite
	Malagrotta waste refusal site	SPF2	R94-30C	Trachyte
Ultra-distal	**Lake Ohrid**	OH-DP-1733	OH-DP-1733	Trachyte

In contrast, it has not been possible to carry out new investigations at Pantano di Grano and Malagrotta (Fig. 2), due to the dismantling of these outcrops by the recent enlargement of the Malagrotta waste refusal site. However, based on the analysis of archive materials (photos, field notes and topographic maps) and the storage of a sample of the Malagrotta layer R94-30C, we could make a critical re-examination of the altimetry, litho-stratigraphic features and glass chemical composition of this tephra.

3.2. Tephrochronological analyses

3.2.1. $^{40}Ar/^{39}Ar$ dating: sampling strategies and analytical procedure

Out of the nine eruptive units, a total of ten samples were selected for $^{40}Ar/^{39}Ar$ dating (Table 1). For the Vico area our aim was to date Vico α (samples VT-1A of Viterbo type locality and CC1-A of Civita Castellana section; Table 1), Vico β (VIG-1top) and the two minor units above Vico β of the Vignanello type locality (VIG-4 and VIG-6), labelled Vico γ and δ, following the nomenclature proposed by Cioni (1993). Finally, for the Roman MIS 11 San Paolo Formation, we selected two samples from the uppermost volcaniclastic unit, labelled SPF4 (sample P1C8 and SC11), two samples of the third volcaniclastic layer SPF3a (P1C7 and SC10B) and one sample of the second volcaniclastic unit SPF3 (P2-C3), from Via della Pisana and Santa Cecilia sections (Table 1 and Fig. 4).

The samples were crushed and sieved to the 500 – 250 μm fraction size. These fractions were then cleaned in distilled water. Magnetic separation allowed the removal of the undesirable magnetic crystals. Unaltered and pristine potassic feldspars (mainly sanidines) were then handpicked under a binocular microscope and ultrasonically leached with a 7 % HF solution for about 5 min to remove potential particles aggregated on the surface of the minerals. Approximately twenty to thirty crystals were selected to produce an age for each sample and were separately loaded into an aluminium disk. Prior to mass spectrometric measurements, samples were activated in two distinct irradiations. All the samples from the San Paolo Formation were irradiated for 90 min (IRR 108) in the β1 tube of the Osiris reactor

(French Atomic Energy Commission, Saclay France). Samples from Viterbo, Vignanello and Civita Castellana were irradiated for 120 min in the Cd-lined, in-core CLICIT facility of the Oregon State University TRIGA reactor (IRR CO002). Interference corrections were based on the nucleogenic production ratios given in Guillou et al., (2018) for Osiris and Renne et al. (2015) for CLICIT. After irradiation, samples were transferred into a copper sample holder and loaded individually into a differential vacuum Cleartan© window. Full and detailed analytical procedures can be found in Nomade et al. (2010). Minerals were fused one by one using a 25 Watts Synrad CO_2 laser at about 10 to 15 % of the nominal power. Extracted gas were then purified for 10 min by two hot GP 10 and two GP 50 getters (ZrAl). Argon isotopes (^{40}Ar, ^{39}Ar, ^{38}Ar, ^{37}Ar and ^{36}Ar) were successively measured using a VG 5400 mass spectrometer equipped with an electron multiplier (Balzer SEV 217 SEN) coupled with an ion counter. Each argon isotope measurement consisted of 20 cycles of peak-hopping. Neutron fluence J for each sample was calculated using co-irradiated Alder Creek sanidine standard (ACs at 1.1891 Ma, Niespolo et al., 2017) and the K total decay constant of Renne et al. (2011). For IRR 108 standards were placed in the same pit as the unknown ones while for IRR CO002 they were placed in three small pits surrounding the samples. This calibration allows to produce ages independent of the astronomical tuning. For irradiation IRR 108 J-values were computed from monitor flux standards co-irradiated with each dated sample (P1C7: J = 0.000396998 ± 0.00000199; P1C8: J = 0.0004006858 ± 0.00000210; P2C3: J = 0.000390412 ± 0.00000118; SC10B: J = 0.0003974963 ± 0.00000120; SC11: J = 0.000400088 ± 0.00000201; for irradiation CO 002 J-values are the followings: VT-1A: J = 0.00053000 ± 0.00000122, Vig-1 Top: J = 0.00053250 ± 0.00000144; Vig-4: J = 0.00053400 ± 0.00000117; Vig-6: J= 0.00053510 ± 0.00000086; CC1-A: J=0.00053500 ± 0.00000107). Mass discriminations was monitored by analysis of air pipette throughout the analytical period, and relative to a $^{40}Ar/^{36}Ar$ ratio of 298.56 (Lee et al., 2006). Procedural blank measurements were achieved after every two or three unknown samples. For typical 10 minutes times of isolation typical backgrounds are about 2.0-3.0 x 10^{-17} and 5.0 to 6.0 x 10^{-19} moles for ^{40}Ar and ^{36}Ar, respectively.

3.2.2. Tephra composition: Major and minor elements glass geochemistry

For the geochemical fingerprinting of the main eruptive units of the early activity of the Vico volcano and other Latium volcanic sources, major and minor oxide element compositions were determined on 35 samples of micro-pumice fragments and/or glass shards. These samples were extracted from 23 individual tephra deposits related to 13 eruptive units, collected in 10 sections in both proximal and distal settings (Tables 1 and 2; Figs. 1, 3 and 4).

Specifically, we analysed:

1) ***In proximal-mid distal area of the Vico volcano***: Pre-Vico α from Viterbo, Vignanello and Civita Castellana sections (Table 1, Fig. 3); Vico α from Viterbo, Vignanello and Civita Castellana sections (Table 1, Fig. 3); Vico β, Vico β_{top}, Vico γ and Vico δ from Vignanello and Civita Castellana sections (Table 1, Fig. 3).
2) ***In the Roman MIS 11 aggradational succession of the San Paolo Formation***: The uppermost volcaniclastic layer SPF4 (Fig. 2) sampled at Via della Pisana 1 and 2 and Santa Cecilia sections; the previously unrecognized volcanic layer SPF3a occurring in-between SPF4 and SPF3, at Via della Pisana 2 section (Fig. 4); the layer SPF3 at Via della Pisana 2, the layer SPF2 of Malagrotta waste refusal site (sample R94-30C, Fig. 2) and the stratigraphically not well defined layer from Foro di Cesare section (Table 1, Fig. 2). No samples of the first volcaniclastic layer SPF1 dated to 436.5 ± 6.1 ka (Marra et al., 2016) was preserved.
3) ***In ultra-distal setting***: The tephra OH-DP-1733 occurring at MIS 12-MIS 11 transition of the paleoclimatic-environmental record of Ohrid Lake (Leicher et al., 2019).

Polishing and carbon coating of the epoxy slides were performed for electron-probe micro analyser wavelength dispersive spectroscopy (EPMA-WDS) analysis at the Istituto di Geologia Ambientale e Geoingegneria of the Italian National Research Council (IGAG-CNR, Rome). Major and minor element quantitative analyses were performed with a CAMECA SX-50 equipped with five wavelength dispersive spectrometers (WDS). The machine operated at 15 kV (operating voltage) and 15 nA (beam current). The standards used for the analyses were: jadeite (for Na), periclase (Mg), orthoclase (K), rutile (Ti), barite (S), wollastonite (Si and Ca), corundum (Al), rhodonite (Mn), phlogopite (F), halite (Cl), magnetite (Fe) and apatite (P). TAP, PET and LIF were employed as analyzing crystals, respectively for Na, Mg, Si, Al and F (TAP), K, Ti, S, Ca, Cl and P (PET), Mn and Fe (LIF).

4. RESULTS

4.1 Lithostratigraphy

4.1.1. Proximal and mid-distal sections of the early Vico explosive activity

Remark on the units' nomenclature

In agreement with the observations of Cioni et al. (1987), additionally to Vico α and β eruptive units, we recognized further distinct minor eruptive units that occur below Vico α, in between Vico α and Vico β and above Vico β. Following the codification based on the Greek alphabet proposed by Cioni et al. (1987, see also Cioni, 1993), we termed these units pre-Vico α, Vico γ and Vico δ.

Viterbo section

This Vico proximal section (Figs. 1 and 3) is one of the type localities of the Vico α eruptive succession described by Cioni et al. (1987), for which a $^{40}Ar/^{39}Ar$ age of 419.0 ± 6.0 ka (2σ uncertainties) was retained based on the step heating analysis of one single sanidine (Laurenzi and Villa, 1987; sample V85-75).

Here, we also recognized the Pre-Vico α unit lying in the pedogenized horizon immediately below the basal Vico α Plinian fall. The general lithostratigraphic features of this section are described in supplementary material S1 and summarized in Figure 3.

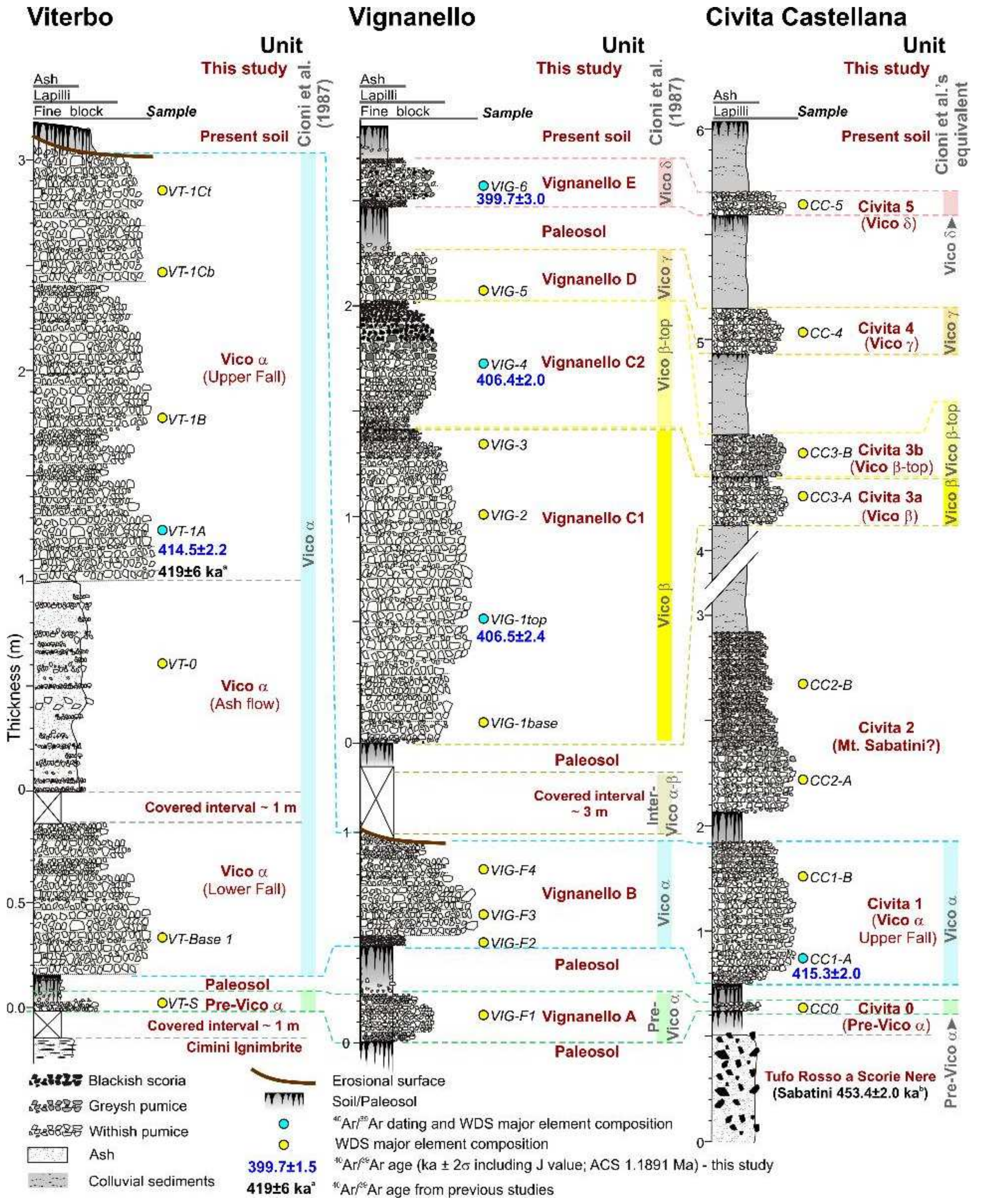

Figure 3. Stratigraphic successions of the Vico α and Vico β Plinian pumice fall deposits and of the minor eruptive units outcropping at Viterbo, Vignanello and Civita Castellana sections (see Fig. 1 for locations). The stratigraphic positions of the samples used for determining the glass geochemical composition and for the $^{40}Ar/^{39}Ar$ dating are also shown. Source of previous $^{40}Ar/^{39}Ar$ ages: [a]Laurenzi and Villa (1987); [b]Karner et al. (2001).

Vignanello section

This section is another type locality documenting the complete early explosive activity of the Vico volcano (Cioni et al., 1987), including Vico α and Vico β and other minor eruptive units. Unfortunately, the current general condition of exposure of this section, largely affected by vegetation and colluvial covering, did not allowed us to observe the whole pyroclastic succession as described by Cioni et al. (1987). In any case, the lowermost part, (including the pre-Vico α and the base of Vico α), and the middle to uppermost part (including Vico β and post-Vico β units) of the Vico activity have been successfully recognized. Only the upper part of Vico α and the minor pyroclastic unit in-between Vico α and Vico β (inter-Vico α–β in Fig. 3) were not observed.

We identified six distinct pumice fall deposits separated by either well-developed or incipient paleosols (Fig. 3). Their general lithostratigraphic features are described in supplementary material S1 and summarized in Figure 3.

Civita Castellana

This section is located within the dispersal area of Vico β Plinian fall, close to the 60 cm contour-line of the Vico β isopach map of Cioni et al. (1987) (Fig. 1a). It exposes a ~6 m thick succession consisting of seven eruptive units (labelled CC0, CC1, CC2, CC3-A, CC3-B, CC4 and CC5), separated by either paleosols or faintly pedogenized colluvial deposits. This thick succession overlies the pyroclastic flow deposits of the Tufo Rosso a Scorie Nere (TRSN) from the Sabatini volcanic district dated to 453.4 ± 2.0 ka (2σ uncertainties, recalculated from Karner et al., 2001) (Fig. 3). Based on the stratigraphic order and diagnostic lithological features of these pyroclastic units, we recognised here the whole succession of Vico units identified at Vignanello type locality: i.e., the series comprised between Pre-Vico α and Vico δ, plus an additional unit in-between Vico α and Vico β, not exposed at Vignanello (Fig. 3). The general lithostratigraphic features of this section are described in supplementary material S1 and summarized in Figure 3.

4.1.2 Ponte Galeria - San Paolo Formation sections

Santa Cecilia, Via della Pisana and Malagrotta waste refusal site sections – The Santa Cecilia section is one of the previously investigated type localities of the MIS 11 aggradational succession of the San Paolo Formation (Marra et al. 2016; Fig. 2). It consists of a ~5 m-thick succession made of whitish lagoonal-marshly silt deposits (carbonatic muds) turning upward to brownish silty deposits affected by diffuse pedogenetic features.

Three sub-primary volcaniclastic layers are intercalated in the succession (Fig. 4), the lowermost of which corresponding to the layer SPF3 or the Ponte Galeria Bedded-Pumice (C7 in Marra et al., 2016), dated at 413.5 ± 2.0 ka (2σ uncertainties) by Karner et al. (2001), and the uppermost undated layer SPF4 (Figs. 2 and 4). A third, previously unreported, volcaniclastic layer has been identified in this study and labelled SPF3a, as it occurs in-between SPF4 and SPF3 (Fig. 4). The same lithostratigraphic succession, characterized by the occurrence of these three distinctive volcanic layers, constitutes the uppermost portion of the hills in this area and is exposed at the two sections in Via della Pisana 1 and 2 investigated in the present study.

Although no longer observable on field, here we also reappraise the actual elevation at which the tephra SPF2 (R94-30C) layer was collected. Indeed, despite previous studies indicated an elevation of ca. 32 m a.s.l. (Marra et al., 2016), the results of the archive data re-examination suggest an elevation of 48 ± 1 m a.s.l, which is closer to the elevation of the San Paolo Formation observed at the Via della Pisana and Santa Cecilia sections (Fig. 4). Notably, the higher elevation of this marker within the sedimentary package of the San Paolo Formation has significant implication on the MIS 11 aggradational model.

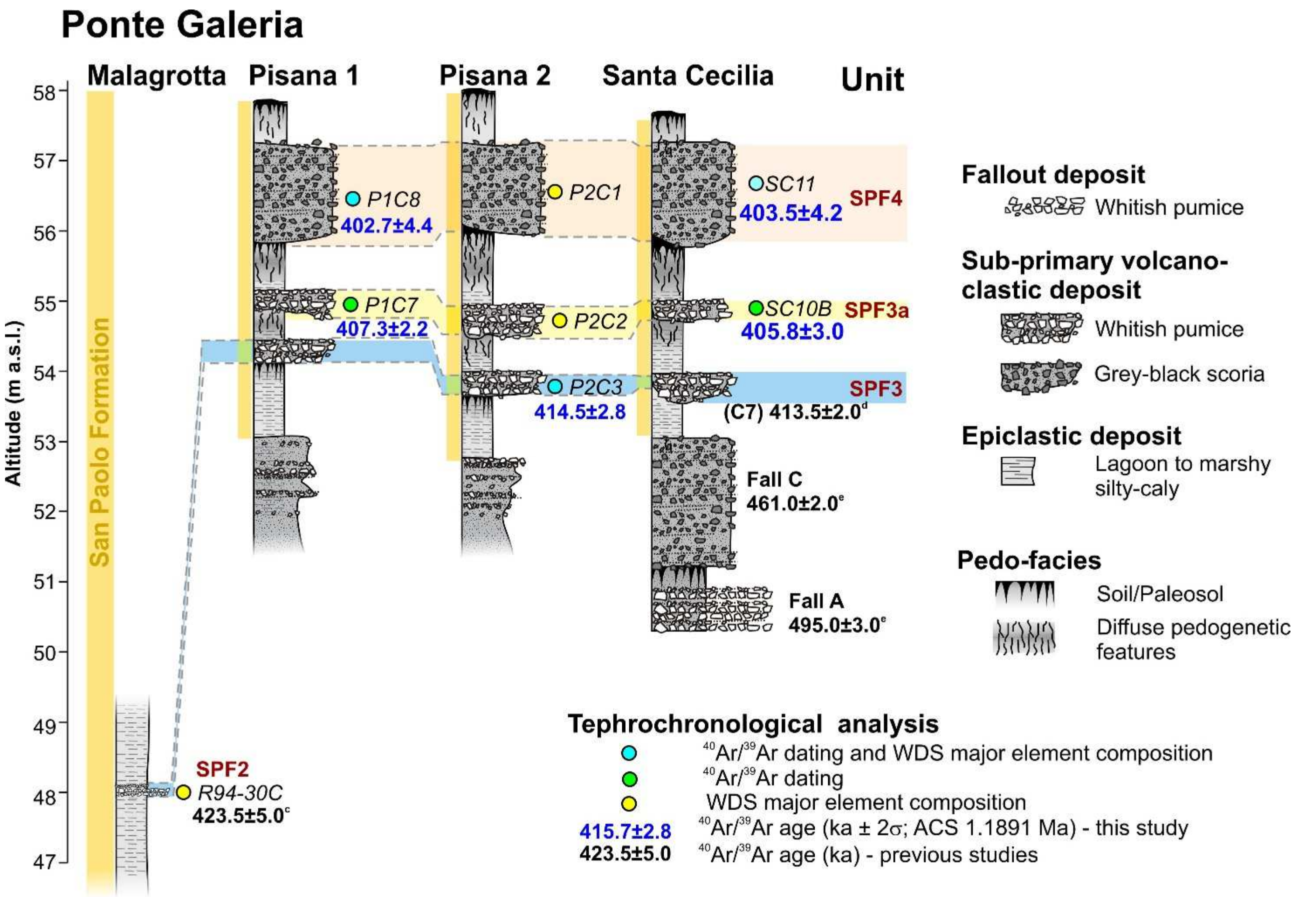

Figure 4. Stratigraphic logs of the investigated sections of the Ponte Galeria area (see Fig. 1 for sections locations). The stratigraphic positions of the samples used for determining the glass geochemical composition and ^{40}Ar/^{39}Ar analyses are also shown. Source of the literature ^{40}Ar/^{39}Ar age: [c]Karner and Renne (1998), [d]Karner et al. (2001); [e]Marra et al. (2017a).

More details on the litho-pedostratigraphic features of these sections are provided in supplementary material S1.

4.2. ^{40}Ar/^{39}Ar single grain analyses

Remark on ^{40}Ar/^{39}Ar age calibration

Since all the ages reported here are obtained using the ^{40}Ar/^{39}Ar method, errors are the analytical uncertainties at 95.5% of confidence (J-value included). Detailed analytical data are available in supplementary data tables S2 to S11 and reported according to the optimized K total decay constant of Renne et al. (2011) and the monitor flux standard ACs-2 at 1.1891 Ma (Niespolo et al., 2017). ^{40}Ar/^{36}Ar initial ratio is quoted at 2σ analytical uncertainties. Results for each dated layer are presented as probability diagrams Figure 5.

4.2.1. Vico volcano area

Vico α – 414.8 ± 2.2 ka

Viterbo (sample VT-1A, Fig. 3) - Twelve crystals of sanidine were individually analysed. Related probability diagram presented in Figure 5 shows a unimodal distribution with only one xenocrystal being 429 ka old (Fig. 5 and table S2). The major population (eleven crystals) defines a weighted mean age of 414.5 ± 2.2 ka, Mean Square Weighted Deviation (MSWD) = 0.9 and Probability (P) = 0.5. The spread along the inverse isochron diagram is very restricted because all the crystals have very similar ^{40}Ar/^{36}Ar and ^{39}Ar/^{40}Ar ratios. Therefore, the inverse isochron intercept is very unprecise (see table S2). It is then impossible to state undoubtedly that this age is unaffected by excess or argon loss.

Civita Castellana (sample CC1-A. Fig. 3 and table S3) - Eleven sanidine crystals have been individually analysed. The bimodal distribution of the ages shows juvenile crystals and a xenocrystic contamination. The youngest population, related to the Vico α eruption is the dominating population (8/11 crystals) with a weighted mean age of 415.3 ± 2.0 ka, MSWD = 0.8 and P= 0.6. The oldest one (3/11 crystals) is instead dated to 424.0 ± 3.4 ka. The ^{40}Ar/^{36}Ar initial ratio calculated for the isochron formalism (i.e., 302.5 ± 21.4, see table S3) is not precise but consistent with atmospheric ratio of 298.56 (Lee et al., 2006).

Because both samples belong to the same pyroclastic event (i.e. Vico α) we combined the data, using a classical inverse variance-weighted average, and obtained for these two samples in the ArArCalc software (v2.5.2, 2012, Koppers, 2002) and calculated an age of 414.8 ± 2.2 ka (including 19 of the 23 crystals dated) for Vico α.

Vico β - 406.5 ± 2.4 ka

Vignanello (sample VIG-1 Top, Fig. 3, table S4) - Eleven sanidine crystals were dated (Fig. 5). All the grains belong to the same population with a resulting unimodal probability diagram characterized by a Gaussian distribution. The related weighted mean age calculated is 406.5 ± 2.4 ka, MSWD = 1.2 and P= 0.3. The $^{40}Ar/^{36}Ar$ initial ratio of 293.6 ± 5.2 (see table S4, 2σ analytical uncertainties) is equivalent to the atmospheric one (table S4).

Vico β_{top} - 406.4 ± 2.0 ka

Vignanello (sample VIG-4, Fig. 3, table S5) - A total of nine sanidine crystals were individually dated. The related probability diagram shown is unimodal (Figure 5) with all the analysed crystals sharing the same age within uncertainties. The weighted mean age calculated is 406.4 ± 2.0 ka, MSWD = 0.5 and P = 0.8. The $^{40}Ar/^{36}Ar$ initial ratio given by the inverse isochron of 296.5 ± 6.0 (table S5) is equivalent within uncertainties to the atmospheric ratio of 298.56 (Lee et al., 2006).

Vico δ - 399.7 ± 3.0 ka

Vignanello (sample VIG-6, Fig. 3, table S6) - A total of ten crystals were measured. Except for one xenocryst, all the grains yielded the same weighted mean age within uncertainties. The calculated related weighted mean age is 399.7 ± 3.0 ka, MSWD = 0.4 and P= 0.9. The $^{40}Ar/^{36}Ar$ initial ratio given by the inverse isochron, slightly imprecise (302.2 ± 12.2, see table S6) is equivalent within uncertainties to the atmospheric one confirming the absence of argon excess.

4.2.2. San Paolo Formation

SPF3 414.5 ± 2.8 ka

Via della Pisana 2 (sample P2C3, Fig. 4, table S7) - A total of twelve crystals were individually dated. The related probability diagram (Figure 5) is multimodal but dominated by a main population of 9 out of 12 dated crystals. The weighted mean age calculated for the main mode is 414.5 ± 2.8 ka, MSWD =

0.5 and P = 0.9. The $^{40}Ar/^{36}Ar$ initial ratio given by the inverse isochron of 304.3 ± 12.6 (table S7) is equivalent within uncertainties to the atmospheric ratio.

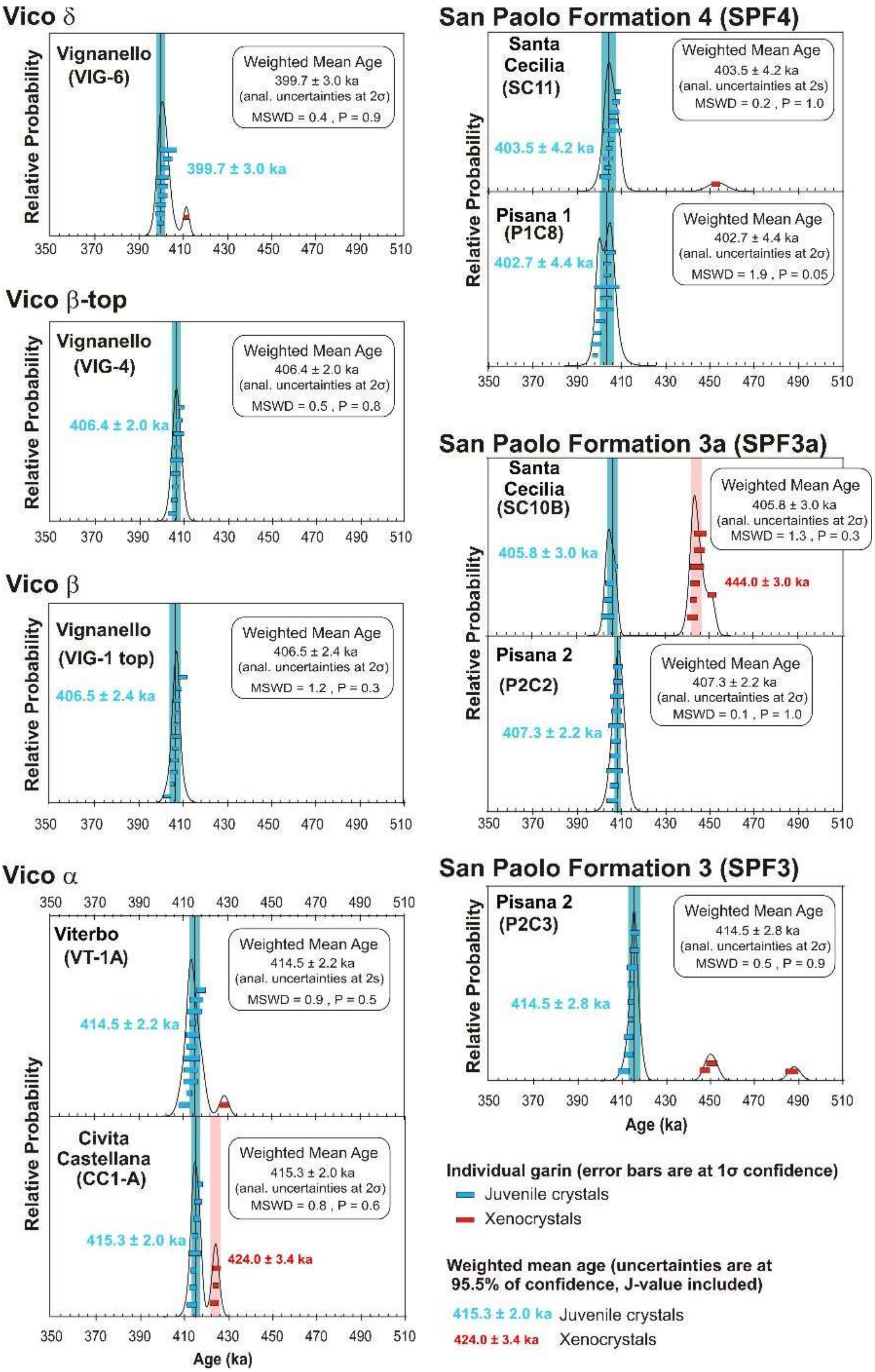

Figure 5. $^{40}Ar/^{39}Ar$ on single grain results (sanidine crystals) presented as probability diagrams.

SPF3a - **406.5 ± 2.5 ka**

Via della Pisana 1 (sample P1C7, Fig. 4, table S8) - A total of ten sanidine crystals were individually dated. The related probability diagram is unimodal and characterized by a Gaussian distribution testifying the homogeneity of the crystal population (Fig. 5). The related weighted mean age calculated is 407.3 ± 2.2 ka, MSWD = 0.1 and P = 1.0. The $^{40}Ar/^{36}Ar$ initial ratio is imprecise (305.4 ± 37.8, see table S8) but similar within uncertainties to the atmospheric ratio.

Santa Cecilia (sample SC10B, Fig. 4, table S9) - Eleven sanidine crystals were individually dated. The related probability diagram is bimodal (Fig. 5). The main population of seven crystals, corresponds to the reworking of an old eruption dated around 445 ka. The juvenile population is represented by four crystals with a weighted mean age of 405.8 ± 3.0 ka, MSWD = 1.3 and P = 0.3. Despite the $^{40}Ar/^{36}Ar$ initial ratio of 318.2 ± 20.5 given by the inverse isochron is imprecise it is equivalent within uncertainties to the atmospheric one of 298.56 (see table S9).

The combined age of SPF3 is 406.5 ± 2.5 ka (14/21 crystals dated, MSWD = 0.5, J-value included).

SPF4 - 403.5 ± 4.2 ka

Via della Pisana 1 (sample P1C8, Fig. 4, table S10) - Ten sanidine crystals were analysed. The related probability diagram is unimodal even if the probability obtained is low P= 0.05 and could thus suggest a mixing among multiple volcanic events very close in age (Fig. 5). The related weighted mean age calculated is 402.7 ± 4.4 ka, MSWD = 1.9. The $^{40}Ar/^{36}Ar$ initial ratio of 324.3 ± 19.4 (table S10) is imprecise, due to the impossibility to define a real slope as all the crystals are characterized by close $^{39}Ar/^{40}Ar$ ratio.

Santa Cecilia (sample SC11, Fig. 4, table S11) - Eleven crystals were individually dated. The related probability diagram presented in Figure 5 is unimodal. Only one xenocryst dated around 452 ka was included within the analysed samples (Fig. 5). The main population of ten crystals has a weighted mean age of 403.5 ± 4.2 ka, MSWD = 0.2 and P = 1.0. The $^{40}Ar/^{36}Ar$ initial ratio given by the inverse isochron is 299.8 ± 6.6 (see table S11), equivalent within uncertainties to the atmospheric one of 298.56, confirming the absence of argon excess of argon fractioning.

The combined age of SPF4 is **403.5 ± 4.2 ka** (20/21 crystals dated, MSWD = 0.7, J-value included).

4.3. Glass chemical composition

4.3.1. General compositional features

Full glass compositions of both proximal and distal analysed pyroclastic deposits are provided in supplementary dataset S12, average compositions are shown in Tables 3, while their classification according to the total alkali versus silica diagram (TAS, Le Maitre, 2002) is shown in Figure 6.

Table 3. Representative major element compositions (average ± 1σ standard deviation; s.d.) of the glass from the near-source pyroclastic sections investigated in this study (see Fig. 1 for sites locations). The full analytical data for the individual glass measurements are provided in supplementary dataset S12.

Unit	**Pre-Vico α**						**Vico α**					
Sub-unit	//						***Lower Fall***					
Glass type	Phonolite						Rhyolite				Trachyte	
Locality	Viterbo		Civita Castellana		Vignanello		Viterbo		Vignanello		Viterbo	
N° analyses	14	*s.d*	13	*s.d.*	15	*s.d.*	8	*s.d.*	29	*s.d.*	8	*s.d.*
SiO_2	59.88	*0.17*	59.83	*0.23*	59.98	*0.21*	72.64	*0.21*	72.72	*0.13*	64,97	*1,28*
TiO_2	0.50	*0.04*	0.53	*0.04*	0.52	*0.03*	0.21	*0.03*	0.22	*0.02*	0,43	*0,04*
Al_2O_3	19.28	*0.12*	19.20	*0.10*	19.25	*0.12*	14.39	*0.07*	14.40	*0.07*	17,48	*0,58*
FeO	2.76	*0.13*	2.94	*0.17*	2.86	*0.14*	1.20	*0.05*	1.25	*0.05*	2,25	*0,29*
MnO	0.18	*0.03*	0.19	*0.05*	0.19	*0.04*	0.08	*0.03*	0.08	*0.04*	0,12	*0,04*
MgO	0.34	*0.03*	0.38	*0.05*	0.35	*0.05*	0.12	*0.01*	0.13	*0.01*	0,33	*0,06*
CaO	2.97	*0.12*	3.05	*0.18*	2.97	*0.12*	1.23	*0.02*	1.21	*0.05*	2,30	*0,17*
Na_2O	4.28	*0.24*	4.46	*0.29*	4.40	*0.37*	3.10	*0.14*	3.22	*0.09*	3,26	*0,19*
K_2O	9.75	*0.38*	9.37	*0.46*	9.44	*0.52*	7.00	*0.19*	6.77	*0.14*	8,84	*0,38*
P_2O_5	0.05	*0.03*	0.04	*0.02*	0.04	*0.02*	0.02	*0.01*	0.01	*0.02*	0,03	*0,02*
F	0.40	*0.11*	0.41	*0.10*	0.37	*0.16*	0.29	*0.07*	0.35	*0.11*	0,33	*0,08*
Cl	0.14	*0.01*	0.15	*0.03*	0.15	*0.03*	0.15	*0.02*	0.15	*0.02*	0,10	*0,03*
SO_3	0.19	*0.07*	0.16	*0.05*	0.16	*0.04*	0.03	*0.03*	0.04	*0.03*	0,07	*0,03*
Analytic tot.	95.27	*0.46*	94.47	*0.58*	95.06	*1.28*	94.89	*0.88*	94.95	*0.27*	64,97	*1,28*
Unit	**Vico α**											
Sub-unit	***Ash Flow***				***Upper Fall***							
Glass type	Rhyolite		Trachyte		Rhyolite				Trachyte			
Locality	Viterbo		Viterbo		Viterbo		Civita C.		Viterbo		Civita C.	
N° analyses	15	*s.d.*	5	*s.d.*	33	*s.d.*	22	*s.d.*	25	*s.d*	30	*s.d.*
SiO_2	72.11	*0.97*	66.45	*2.00*	72.48	*0.73*	72.63	*0.21*	60.89	*0.66*	62.12	*0.33*
TiO_2	0.21	*0.02*	0.30	*0.07*	0.21	*0.03*	0.20	*0.03*	0.47	*0.04*	0.43	*0.03*
Al_2O_3	14.63	*0.45*	17.22	*0.98*	14.47	*0.31*	14.52	*0.12*	18.23	*0.20*	18.24	*0.11*
FeO	1.33	*0.31*	1.85	*0.25*	1.27	*0.11*	1.24	*0.06*	3.42	*0.25*	2.94	*0.11*
MnO	0.08	*0.03*	0.07	*0.02*	0.08	*0.04*	0.07	*0.04*	0.21	*0.51*	0.11	*0.04*
MgO	0.15	*0.11*	0.19	*0.04*	0.12	*0.02*	0.12	*0.01*	0.65	*0.08*	0.51	*0.03*
CaO	1.33	*0.42*	2.19	*0.62*	1.22	*0.08*	1.22	*0.04*	3.27	*0.21*	2.80	*0.09*
Na_2O	2.95	*0.24*	2.85	*0.22*	3.09	*0.15*	3.07	*0.17*	2.62	*0.11*	2.82	*0.14*
K_2O	7.19	*0.26*	8.84	*0.75*	7.05	*0.22*	6.90	*0.19*	10.14	*0.33*	9.95	*0.19*
P_2O_5	0.02	*0.02*	0.05	*0.04*	0.01	*0.02*	0.02	*0.02*	0.12	*0.03*	0.08	*0.03*
F	0.26	*0.13*	0.27	*0.11*	0.36	*0.12*	0.37	*0.10*	0.28	*0.12*	0.28	*0.10*
Cl	0.13	*0.02*	0.11	*0.04*	0.14	*0.03*	0.14	*0.02*	0.06	*0.02*	0.07	*0.02*
SO_3	0.02	*0.02*	0.04	*0.03*	0.02	*0.02*	0.02	*0.02*	0.08	*0.03*	0.05	*0.03*
Analytic tot.	96.09	*1.03*	96.27	*1.66*	95.35	*0.80*	95.80	*0.80*	95.79	*1.05*	95.34	*1.16*
Unit	**Vico β**								**Vico β_{top}**			
Glass type	Rhyolite				Trachyte				Trachyte (main composition)			
Locality	Vignanello		Civita C.		Vignanello		Civita C.		Vignanello		Civita C.	
N° analyses	87	s.d.	18	s.d.	1	s.d.	2	s.d.	29	s.d.	13	s.d.
SiO_2	74.22	*0.62*	74.26	*0.28*	60.09		62.07	*0.09*	59.84	*0.58*	60,24	*0,81*
TiO_2	0.13	*0.03*	0.14	*0.02*	0.56		0.52	*0.01*	0.54	*0.03*	0,54	*0,05*
Al_2O_3	13.85	*0.31*	13.85	*0.16*	18.50		17.78	*0.03*	18.28	*0.32*	18,27	*0,24*
FeO	1.13	*0.15*	1.13	*0.11*	3.41		3.17	*0.22*	3.89	*2.23*	3,65	*0,27*
MnO	0.09	*0.03*	0.09	*0.03*	0.15		0.09	*0.07*	0.12	*0.04*	0,12	*0,04*
MgO	0.08	*0.01*	0.07	*0.01*	0.70		0.56	*0.02*	0.94	*0.09*	0,86	*0,09*
CaO	1.04	*0.09*	1.04	*0.08*	3.41		3.18	*0.00*	4.04	*0.54*	3,75	*0,22*
Na_2O	3.19	*0.19*	3.23	*0.14*	3.11		3.13	*0.26*	2.79	*0.21*	2,86	*0,12*
K_2O	6.26	*0.28*	6.19	*0.20*	9.96		9.37	*0.13*	9.36	*0.90*	9,54	*0,33*
P_2O_5	0.01	*0.02*	0.01	*0.01*	0.11		0.13	*0.07*	0.20	*0.03*	0,16	*0,03*
F	0.58	*0.13*	0.53	*0.14*	0.24		0.38	*0.07*	0.29	*0.12*	0,32	*0,10*
Cl	0.22	*0.02*	0.21	*0.02*	0.11		0.10	*0.01*	0.07	*0.02*	0,09	*0,01*

SO_3	0.02	*0.02*	0.03	*0.02*	0.25		0.23	*0.10*	0.20	*0.10*	0,21	*0,05*
Analytic tot.	94.81	*1.19*	95.98	*0.47*	94.38		95.69	*0.78*	95.39	*1.17*	94,87	*0,92*
Unit	**Vico γ**						**Vico δ**				**Sabatini CC2**	
Glass type	Trachyte				Rhyolite		Trach.-Phono.		Trach.-Phono.		Phonolite	
Locality	Vignanello		Civita C.		Civita C.		Vignanello		Civita C.		Civita C.	
N° analyses	21	*s.d.*	4	*s.d.*	8	*s.d.*	37	*s.d.*	15	*s.d*	17	*s.d.*
SiO_2	62.67	*2.81*	65.05	*3.58*	71.13	*0.32*	59.50	*0.57*	60.09	*0.81*	57.51	*0.37*
TiO_2	0.50	*0.13*	0.39	*0.08*	0.26	*0.03*	0.55	*0.04*	0.53	*0.03*	0.50	*0.05*
Al_2O_3	17.63	*1.20*	16.21	*1.00*	14.50	*0.15*	18.48	*0.17*	18.44	*0.21*	20.08	*0.19*
FeO	3.50	*0.97*	2.92	*0.71*	1.51	*0.04*	3.84	*0.22*	3.64	*0.28*	3.36	*0.18*
MnO	0.11	*0.05*	0.11	*0.06*	0.08	*0.03*	0.13	*0.04*	0.11	*0.04*	0.15	*0.03*
MgO	0.77	*0.35*	0.58	*0.42*	0.14	*0.01*	0.87	*0.11*	0.79	*0.09*	0.31	*0.05*
CaO	3.67	*1.19*	2.61	*1.67*	1.13	*0.05*	3.67	*0.29*	3.44	*0.28*	4.44	*0.40*
Na_2O	2.98	*0.29*	2.94	*0.10*	3.07	*0.10*	3.03	*0.16*	2.98	*0.10*	4.64	*0.66*
K_2O	8.01	*0.80*	9.11	*0.37*	8.17	*0.44*	9.80	*0.41*	9.84	*0.19*	8.97	*0.91*
P_2O_5	0.16	*0.08*	0.10	*0.09*	0.02	*0.01*	0.14	*0.03*	0.14	*0.03*	0.04	*0.03*
F	0.29	*0.19*	0.40	*0.13*	0.56	*0.09*	0.32	*0.11*	0.31	*0.13*	0.57	*0.08*
Cl	0.08	*0.03*	0.11	*0.01*	0.13	*0.03*	0.09	*0.02*	0.08	*0.01*	0.11	*0.01*
SO_3	0.06	*0.06*	0.09	*0.11*	0.03	*0.02*	0.19	*0.06*	0.16	*0.03*	0.33	*0.12*
Analytic tot.	95.28	*1.53*	95.56	*0.63*	96.59	*0.89*	95.52	*1.21*	96.54	*0.78*	94.86	*0.97*

4.3.2. Geochemical composition of Vico α and Vico β Plinian units and of the minor pre-Vico α and post-Vico β eruptions

Pre-Vico α

Viterbo and Vignanello – The glass composition of Pre-Vico α, sampled at Viterbo, Vignanello and Civita Castellana, is phonolitic and quite homogeneous, with an average of the silica content and alkali sum of 59.9±0.2 wt% and 13.9±0.3 wt% (±1s standard deviation), respectively (Figs. 6a and 7).

Vico α

Viterbo, Vignanello and Civita Castellana - The composition of the glass from Vico α sampled at Viterbo is zoned, ranging from trachyte to rhyolite (Fig. 6b). Specifically, the Lower Fall sub-unit has a scattered trachyte-rhyolite composition, with SiO_2 content ranging between ~64 wt% and ~73 wt% and alkali sum between ~12 wt% and 10 wt% (Figs. 6b and 7). The Flow subunit is instead mainly rhyolitic in composition, with a SiO_2 and alkali sum contents of ~72 wt% and ~10 wt%, respectively, and a lesser trachyte component with scattered SiO_2 and alkali sum contents content ranging between 63 and 68 wt% and 11-12 wt%, respectively (Fig. 7). The lower part of the Plinian Upper Fall subunits (sample VT-1A and VT-1B) has a dominant, quite homogeneous trachytic composition, with ~61-62 wt% of SiO_2 and ~12-13 wt% of alkali sum, with only few glasses, compositions plot in the rhyolitic field (SiO_2 ~72 wt%, alkali sum ~10 wt%), close to the composition of the Flow subunit (Fig. 7). Finally, the uppermost Plinian Upper Fall (VT-1C) has a quite homogeneous rhyolitic composition with silica content mainly clustering around 72-73 wt% and alkali sum of ~10 wt% (Fig. 7).

Pumices clasts from Vico α sampled at Vignanello are instead predominantly rhyolitic in composition, with SiO_2 around 72.5 wt% and alkali sum of ~10 wt% (Figs. 6b and 7). Finally, at Civita Castellana section, Vico α shows a marked bimodal composition, with a trachytic basal part (SiO_2 ~61-63 wt% and alkali sum ~12.5-13.0 wt%) and a rhyolitic upper part (SiO_2 ~72-73 wt% and alkali sum ~10 wt%) (Figs. 6b and 7).

Overall, the composition of Vico α sampled in the three localities, is bimodal with two dominant components, trachyte (SiO_2 61-63 wt%, alkali sum 12-13 wt%) and rhyolite (SiO_2 72-73 wt%, alkali 10-11 wt%), linked to a third component characterized by a scattered intermediate composition with SiO_2 content ranging between 63-71 wt% and alkali sum between 12 and 10 wt% (Figs. 6b and 7).

Considering the upsection textural and geochemical variability of most complete section of Viterbo as the reference, though incomplete, succession of Vico α eruption, the two more incomplete (i.e., Vignanello) or more distal (Civita Castellana), can be tentatively correlated to the Lower Fall and Upper Fall subunits, respectively. However, we notice that the silica content in the trachyte component of Vico α at Civita Castella section is sensibly higher than the trachyte component of the Upper Fall of Viterbo. Considering the analytical precision of the WDS measurements, with errors lesser than 0.3 wt% on silica (see supplementary dataset S12), we are inclined to interpret this as a real geochemical difference and consider the trachyte component of Vico α at Civita Castellana as a unit not recorded at Viterbo, likely because of the different dispersal axes of the Plinian falls during different stages of the eruption fed by compositionally not homogenous magma. However, the number of the investigated sections is too scant for addressing the issue of the eruption dynamics and variability of the magma composition during the eruption, and this interpretation must be considered as a mere hypothesis.

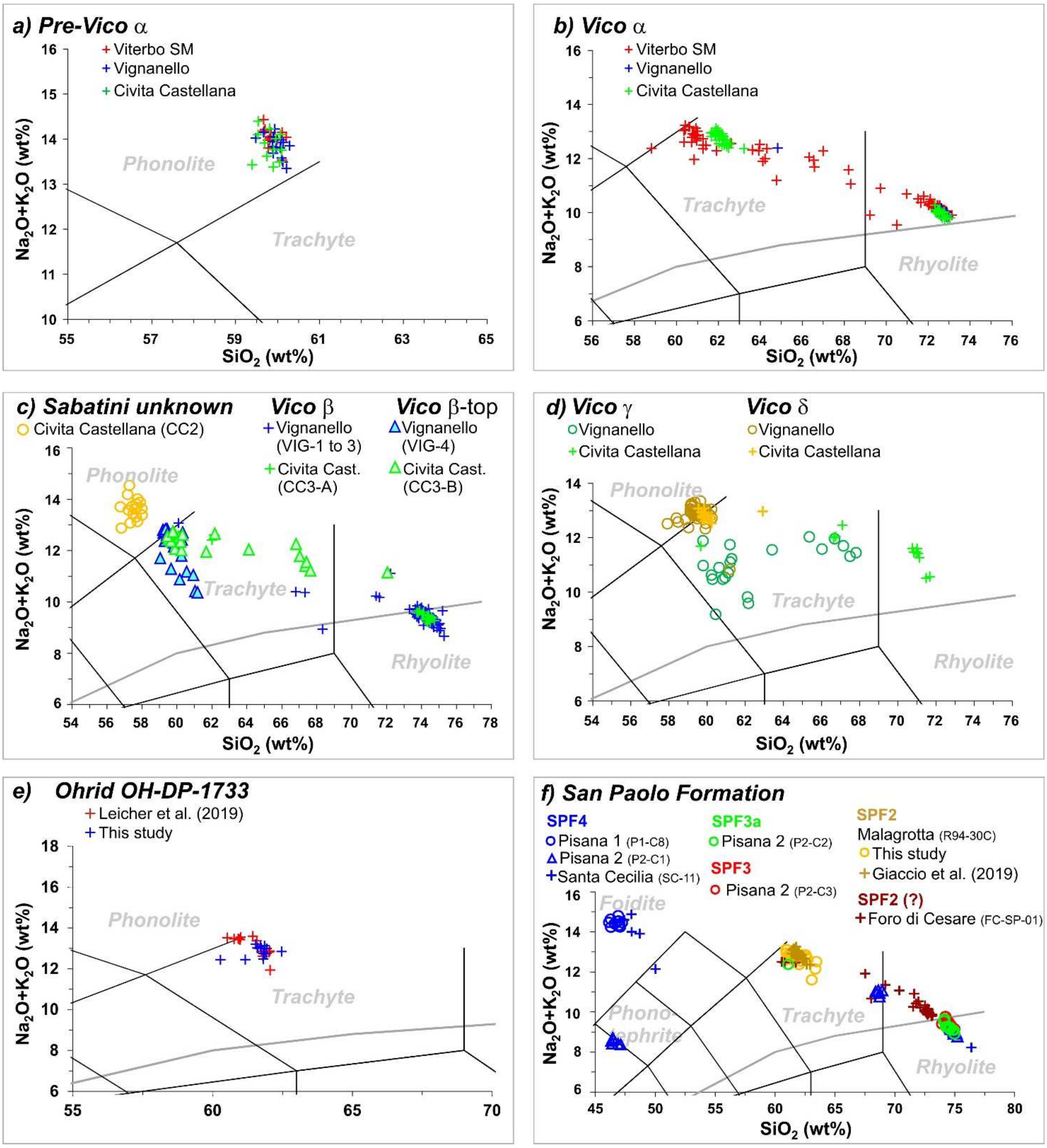

Figure 6. Total alkali versus silica classification diagram (Le Maitre, 2002) of the investigated pyroclastic units and tephras (2σ standard deviations of replicate EMPA-WDS analyses of the Rhyolite RLS132-USGS and Kakanui Augite standards are not shown here as the uncertainties are smaller than the data symbols; see supplementary dataset S12).

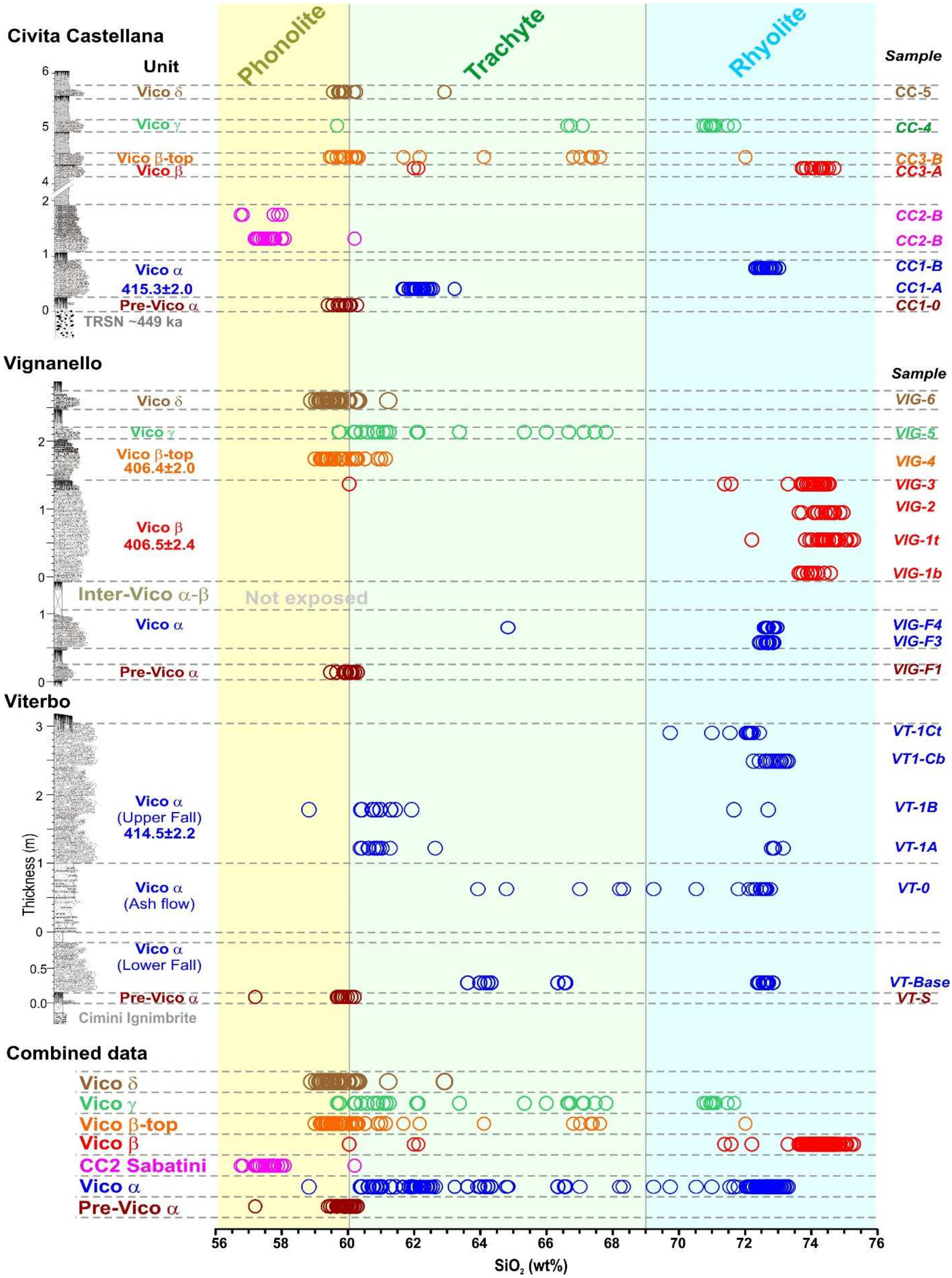

Figure 7. Variation of the silica content upsections within the Vico α and Vico β Plinian eruptions and the minor pre-Vico α and post-Vico β units (2σ standard deviations of replicate EMPA-WDS analyses of the Rhyolite RLS132-USGS and Kakanui Augite standards are not shown here as the uncertainties are smaller than the data symbols).

Sabatini unknown

Civita Castellana CC2 – The glass from this unknown pumice-scoria fallout has a quite homogeneous phonolitic composition, characterized by a SiO_2 content of ~57 wt% and an alkali sum of ~13-14 wt% (Fig. 6c). The Civita Castellana section is in a peripheral area of both Vico and Sabatini volcanoes (Fig. 1b). CC2 pumice fall could thus be equally attributed to Vico or Sabatini. However, considering the diagram Cl vs CaO/FeO for discriminating the volcanic sources of the Italian trachyte, phonolite and tephrophonolite (Giaccio et al., 2019), we notice that the glass from CC2 pumice fall has a content of Cl of 0.11±0.01 wt% (1σ standard deviation) and CaO/FeO ratio of 1.32 ± 0.07, which is well within the field of the Sabatini products and quite far from the Vico one, featured by a sensibly lower CaO/FeO ratio of ~1 (Giaccio et al., 2019). Therefore, CC2 is likely a previously unknown Sabatini eruption.

Vico β

Vignanello C1 and Civita Castellana CC3-A – The glass from unit VIG-C1 at Vignanello, corresponding to Vico β of Cioni et al. (1987), has an almost homogeneous rhyolitic composition with a silica content narrowly ranging 74-75 wt% (Figs. 6c and 7). Only toward the top of the unit VIG-C1 (sample VIG-3), sporadic trachytic and subordinate silica-rich rhyolitic compositions occur (Fig. 7). Also, at Civita Castellana, the unit CC3-A/Vico β has an almost homogeneous rhyolitic composition with very few shards trachytic in composition, as found at Vignanello section (Figs. 6c and 7).

Overall, the composition of Vico β sampled at the two localities, is bimodal with a dominant homogeneous rhyolite population, with SiO_2 ranging around 74-75 wt%, and a subordinate heterogeneous rhyolite-trachyte one with SiO_2 ranging between 72 wt% and 60 wt%.

Vico β_{top}

Vignanello C2 and Civita Castellana CC3-B – The glass from unit C2 at Vignanello (sample VIG-5), immediately lying on the faintly developed paleosol on Vico β of Cioni et al. (1987), has a quite homogeneous trachytic composition, with silica and alkali contents ranging from ~59 to 61 wt% and from 10 to 13 wt%, respectively (Figs. 6c and 7). A similar composition is also found in the unit 3b of Civita Castellana (sample CC3-B), but here Vico β_{top} also shows a more variable trachytic composition with higher silica content, up to 68 wt%, and a rhyolitic component is also documented.

Overall, the composition of Vico β_{top} is quite heterogeneous, with a dominant population with silica at ~59 to 61 wt%, and a second population with a scattered SiO_2 content ranging between ~62 and ~72 wt% (Figs. 6c and 7).

Vico γ

Vignanello D and Civita Castellana CC4 – The glass from unit D at Vignanello, corresponding to Vico γ, has a heterogeneous trachyte composition, with silica and alkali sum ranging ~60-68 wt% and ~9-12 wt%, respectively (Figs. 6d and 7). The corresponding unit at Civita Castellana (CC4) has a similar variable trachytic composition but also shows a rhyolitic component (Figs. 6d and 7).

Vico δ

Vignanello E and Civita Castellana CC5 – The glass from unit E at Vignanello, corresponding to Vico δ has an almost homogeneous composition across the trachyte-phonolite field boundary with ~59-60 wt% of silica and ~13 wt% of alkali sum (Figs. 6d and 7). The same homogeneous trachytic-phonolitic composition was found for the equivalent level CC5 of the Civita Castellana section (Fig. 7).

4.3.3. Geochemical composition of tephra from MIS 11 aggradational successions of the San Paolo Formation

SPF4 – The composition of this volcaniclastic layer (see supplementary material S13 for the lithostratigraphic features) is highly variable, with four well grouped populations of glass clustering in the rhyolite, high-silica trachyte, phonotephrite and foidite fields (Fig. 6f). Specifically, three of these compositions (rhyolite, high-silica trachyte and phonotephrite) coexist in the sample of Via della Pisana 2 section (P2-C1), while at Santa Cecilia we found both the foidite and rhyolite components, and finally at Pisana 1 we only found the foidite component (Fig. 6f).

SPF3a – The fresh glass evidenced in this layer sampled at Via della Pisana 2 section (P2C2), has an almost homogeneous rhyolitic composition characterized by a SiO_2 content of ~75 wt% and an alkali sum of ~9 wt%. Only one glass shard has a trachytic composition with ~62 wt% of silica.

SPF3 – The glass in the pumice clasts from this layer at Via della Pisana 2 section (P2C3) has a homogeneous rhyolitic composition similar to SPF3a (Fig. 6f).

SPF2 – Additional analyses made on the glass from the basal coarser level of the Malagrotta ash fallout (R94-30C; see supplementary material S13 for the lithostratigraphic features) which is characterized by a SiO_2 content of ~62-63 wt% and alkali sum of ~12-13 wt% (Fig. 6f), confirm the previously reported trachytic composition (Giaccio et al., 2019).

SPF2 (?) – This layer (FC-SP-01), of uncertain stratigraphic position within the tephra series of the San Paolo Formation (Fig. 2), shows a wide compositional variability, from trachyte (SiO_2 ~60-62 wt%) to rhyolite (SiO_2 ~72-73 wt%), with sparse intermediate composition (SiO_2 ~67-70 wt%9 (Fig. 6f).

5. DISCUSSION

5.1. Improved chronology and geochemical fingerprint for the early Vico explosive activity

5.1.1. Two proximal chronological markers

Previous knowledges of the chronology of the early Vico eruptive activity were mainly based on two age determinations provided for Vico α (Laurenzi and Villa 1987) and Vico β (Barberi et al., 1994). Regarding the Vico α eruption, the age of 419 ± 6 ka reported in Laurenzi and Villa (1987) is rather imprecise and, above all, relies on the dating of only one sanidine crystal, making the result statistically poorly significant. This age was calibrated against Bern 4 Muscovite standard (B4M, Flisch, 1982), dated to 18.6 Ma and the K total decay constant of Steiger and Jäger, 1977. According to the standardization used in this paper (Renne et al., 2011 and ACs standard dated to 1.1891 Ma, Niespolo et al., 2017), it can be recalibrated to an age of 421.5 ± 6 ka. The new $^{40}Ar/^{39}Ar$ age we obtained combining the dating of Vico α collected at Viterbo and Civita Castellana allows to accurately date this eruptive unit to 414.8 ± 2.2 ka, which is consistent with the age provided by Laurenzi and Villa (1987) and in good agreement with that of 412 ± 2 ka proposed by Marra et al. (2014b) for the sample C7 from Santa Cecilia section, assumed to correlate with Vico α (Karner et al., 2001). Nevertheless, our new age determinations of the main Plinian event (412.6 - 417.0 ka), is significantly more precise compared with the wider interval of 415.6-427.5 ka determined previously.

We also provided an $^{40}Ar/^{39}Ar$ dating for the Vico β Plinian eruption that is stratigraphically above Vico α and sampled at Vignanello (sample Vig-1 Top, see Figs. 1 and 3). Barberi et al. (1994) reported an age of 403.0 ± 6.0 ka (level V88-7/TSVVβ). Unfortunately, because at the time it was not mandatory to specify the $^{40}Ar/^{39}Ar$ calibration used, it prevents us from recalibrating this age according to our preferred calibration. However, the new age of 406.5 ± 2.4 ka we obtained for Vico β is apparently consistent with the previous age and significantly improves the precision and, possibly, the accuracy of the dating of Vico β (Fig. 5).

Moreover, our $^{40}Ar/^{39}Ar$ investigations at Vignanello permit us to constrain the age the minor volcanic events from the upper part of the early Vico eruptive succession. Specifically, the age of 406.4 ± 2.0 ka obtained for Vico β_{top} is statistically indistinguishable from Vico β (Fig. 5), while a substantial younger age of 399.7 ± 3.0 ka was obtained for Vico δ pumice fall, the uppermost recognised unit of the Vico Period I. Though not representing the focus of this paper, these new chronological constraints allows us to precisely define the timing of Vico Period I explosive activity as briefly discussed in the section 5.3.4.

5.1.2. Diagnostic geochemical features of Vico α and Vico β Plinian eruptions

Previous geochemical compositions of the near-vent pyroclastic units from the early explosive activity of Vico volcano were reported by Cioni et al. (1987) and Perini et al. (2004). However, Cioni et al. (1987) only reported whole rock compositions for Vico α and Vico β while Perini et al. (2004), although providing additional whole rock compositions, did not distinguish data for Vico α, Vico β and other minor units, which were grouped in the Rio Ferreira Fm.

Our results provide a precise dataset of the geochemical glass compositions the early eruptive units of Vico volcano, offering the possibility to trace in distal setting these potentially widely dispersed tephra. One of the most distinctive feature of both Vico α and Vico β units, as well as of other minor eruptions of the Vico early activity (Fig. 7), is their K-rhyolitic composition, which is really rare and peculiar within the Italian ultra-potassic Quaternary volcanism (e.g., Peccerillo, 2017). This specific feature makes their potential recognition in distal settings quite straightforward. Nevertheless, distinguishing via geochemical composition the two main events and the minor eruptions might be quite challenging. Although, the bimodal trachyte-rhyolite composition of Vico α could be considered as a distinctive character with respect to the nearly homogeneous rhyolitic composition of Vico β (Fig. 7), the possible concomitant occurrence of the sub-contemporaneous, geochronologically indistinguishable, Vico β (406.4 ± 2.4 ka) and Vico β_{top} (406.4 ± 2.0 ka), might complicate the tephra recognition. Indeed, the trachyte composition of Vico β_{top} is a quite similar to the trachyte component of Vico α, and thus the combination of Vico β and Vico β_{top} mimics the bimodal trachyte-rhyolite composition of Vico α (Fig. 8).

Despite this potential complication, using some specific bi-plots, discriminating Vico α from Vico β-Vico β_{top} could reasonably be feasible. The main geochemical differences are the higher silica content and silica/alkali ratio ($SiO_2/(Na_2O+K_2O)$) of Vico β with respect to the rhyolitic component of Vico α (Fig. 8). Furthermore, the Vico beta rhyolitic glasses show considerably more variability in their CaO/MgO ratios than for the Vico alpha (Fig. 8). The trachytic glasses of the Vico α and Vico β_{top} eruption units can be distinguished based on their MgO content, which is noticeably higher in the Vico β_{top} despite overlapping SiO_2 content. (Fig. 8).

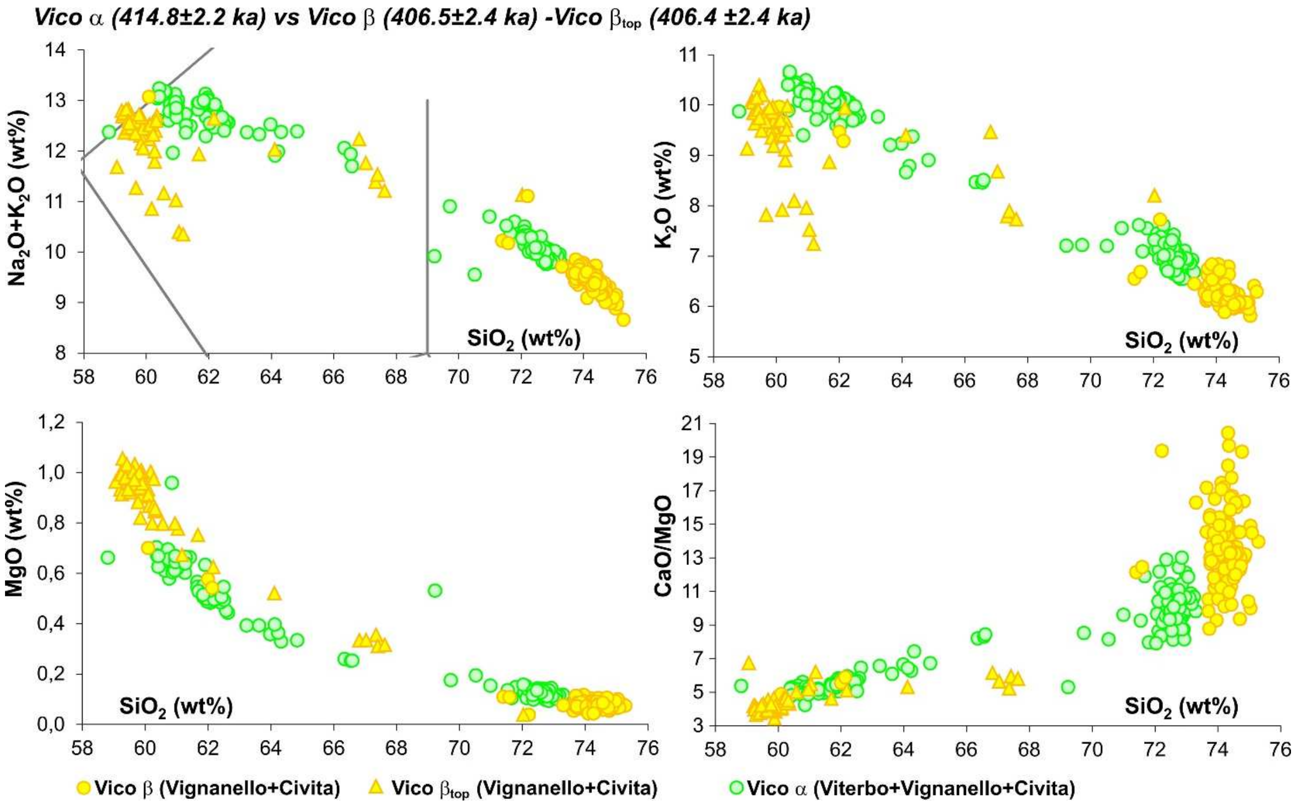

Figure 8. Total alkali versus silica classification diagram (Le Maitre, 2002) and representative bi-blots useful for discriminating the proximal units Vico α, Vico β and Vico β_{top} units.

5.2. Identification of the tephra from the San Paolo Formation

Vico α and Vico β - Five samples from the San Paolo Formation, dated in both previous and present studies, are chronologically consistent with the new ages obtained for either Vico α or Vico β. For Vico α these are: (i) the layer SPF3 of Via della Pisana sections (sample P2-C3), dated here at 414.5 ± 2.8 ka (Fig. 5), (ii) the layer SPF3 of the Santa Cecilia section (sample C7), dated at 413.5 ± 2.0 ka (Karner et al., 2001) and (iii) the layer of uncertain stratigraphic position from Foro di Cesare section (sample FC-SP-01), dated to 419.5 ± 6.0 ka (Marra et al., 2016). For Vico β the chronologically corresponding layer is SPF3a sampled from Via della Pisana 2, (P2C2) and Santa Cecilia (SC10B) sections, for which here we got the age of 407.3 ± 2.2 ka and 405.8 ± 3.0 ka, respectively (Fig. 5). The attribution of SPF3a to Vico β is also supported by a good match of their glass composition (Fig. 9a).

If we consider the ages previously obtained for SPF3, while the high-precision age for SPF3 at Santa Cecilia (sample C7) is in very good agreement with that of Vico α, this is not the case for the layer sampled at Foro di Cesare (FC-SP-01), for which large uncertainties on dating (i.e., ± 6.0 ka) and stratigraphic position persist. However, the glass composition from Foro di Cesare layer precisely matches that of Vico α, supporting their correlation (Fig. 9b). In contrast, while the new age obtained for SPF3 (i.e., P2C3, 414.5 ± 2.8 ka) at Via della Pisana 2 and Vico α, (i.e., 414.8 ± 2.2 ka) are virtually identical, the chemical compositions are not fully consistent. Although the rhyolitic glass composition of SPF3 at Via della Pisana 2 leaves no doubt on its origin from the early Vico activity, it differs significantly from the rhyolite component of Vico α, rather approaching the composition of Vico β or SPF3a (Fig. 9a). Nevertheless, considering the chronological data and the fact that SPF3 of Pisana 2 section (P2C3) is stratigraphically below SPF3a, which is chronologically and geochemically fully consistent with Vico β, we are confident in attributing this layer to Vico α as well. This implies that the SiO_2 content of the rhyolitic component of Vico α might be higher than detected so far in proximal sections, which is possibly documented in the upper 2 m-thick interval of Vico α succession that we missed. Therefore, assuming SPF3 matches Vico α and documents a composition so far not recognised in proximal area for the chemical fingerprinting purposes, we must consider also this SiO_2-richer component. This indeed makes the discrimination between Vico α and Vico β via major element composition quite challenging, as the rhyolite components of these two eruptions become almost indistinguishable (Fig. 9a).

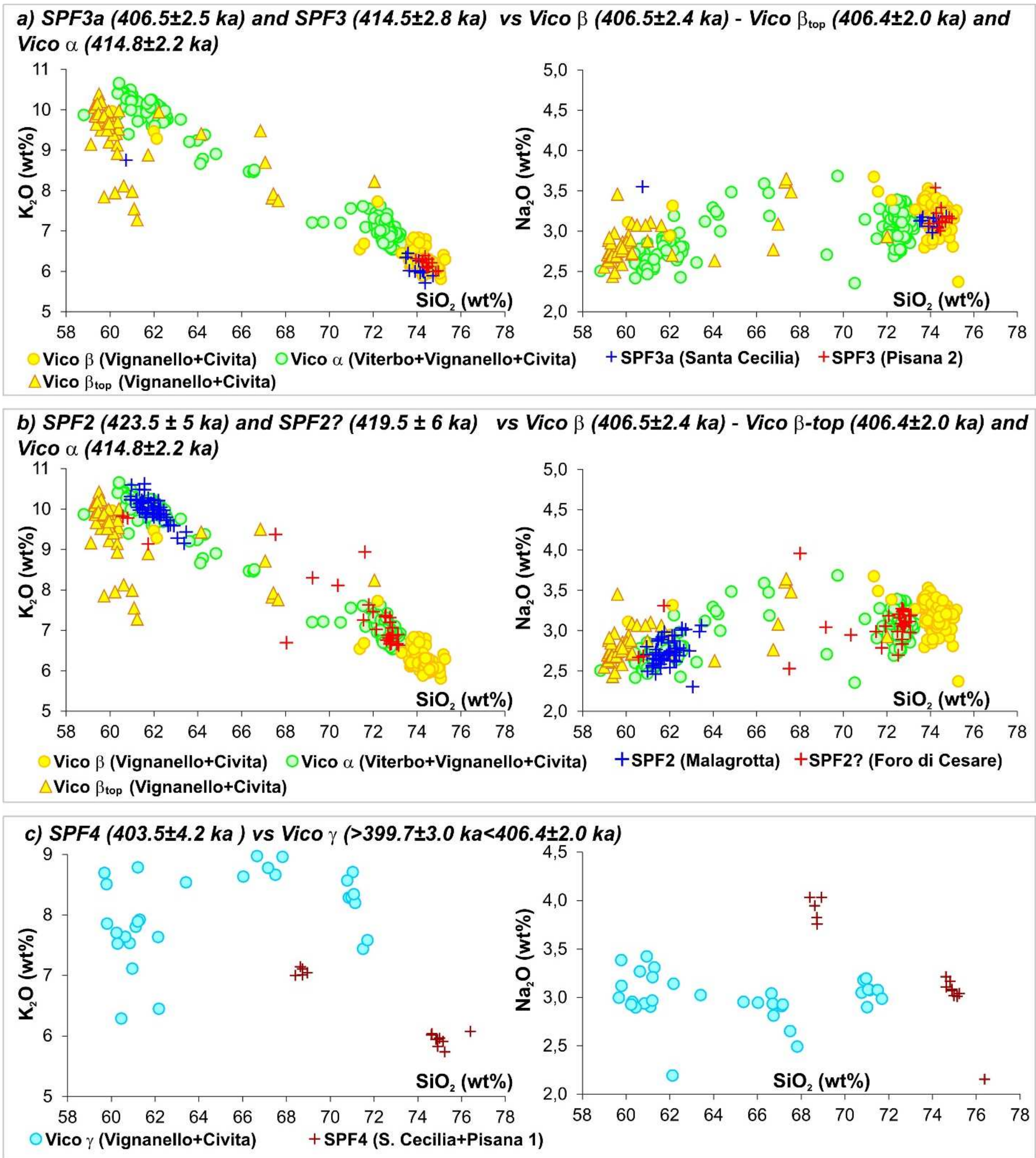

Figure 9. Representative bi-plots used for the comparisons and correlations of the investigated tephra. **a)** Comparison of SPF3a (Santa Cecilia) and SPF3 (Via della Pisana 2) with the Vico α and Vico β-Vico β_{top} proximal units. **b)** Comparison of SPF2 (Malagrotta) and SPF2? (Foro di Cesare) with the Vico α and Vico β-Vico β_{top} proximal units. **c)** Comparison of SPF4 (Santa Cecilia and Via della Pisana 1) with the proximal units Vico γ unit (Vignanello and Civita Castellana). Data source: all the geochemical and geochronological data are from this study.

Regarding layer SPF2 (Fig. 2), the age of 423.5 ± 5.0 ka (Karner and Renne, 1998) would apparently rule out a possible correlation with Vico α, as it is statistically distinct from that of 414.8 ± 2.2 ka, here obtained for Vico α (CC1-A + VT1-A). In spite of this, the chemical composition of the base of SPF2 tephra layer (sample R94-30C) precisely matches that of the trachyte component of Vico α pumice fall, and more specifically that of the basal sub-unit sampled at Civita Castellana (Fig. 10b). It is also worth mentioning that the age calculated by Karner and Renne (1998) for SPF2 (R94-30C) was based on seven crystals and five of them presented uncertainties larger than 25 ka, making the interpretation of this age quite challenging. In addition, the weighted mean age of the xenocrysts (3 out of 11) identified in Vico α at Civita Castellana (424 ± 3.4 ka, Fig 5) is consistent with the age of SPF2. Finally, here we also have shown that the previously reported altitude for SPF2 around ~32 m a.s.l was wrong, and that this layer actually was at ~48-49 m a.s.l. (Fig. 4). When considering the different sedimentary, paleoenvironmental settings of the Malagrotta and Via della Pisana 1-2/Santa Cecilia (i.e., deep lagoon *versus* alluvial plain, respectively) the elevation of SPF2 is consistent with that of SPF3-Vico α (Fig. 11). Therefore, several lines of evidence indicate that SPF2 doesn't exist, and matches SPF3, which in turn is correlated to Vico α. It was erroneously identified as an additional tephra because of (i) its abnormal old age with respect to the other age available for SPF3, likely because of xenocryst contamination as also found in Vico α, and (ii) the misleading elevation of ~32 m a.s.l. that was previously reported for this layer, significantly lower and stratigraphically inconsistent with that of SPF3. A summary of the above proposed tephra correlations is reported in Figure 10.

Other tephra - The polymodal, rhyolitic to high-silica trachytic, foiditic and phonotephritic compositions of the glass from the layer SPF4 capping the San Paolo Formation aggradational succession (Fig. 4), would suggest that it is likely made of reworking and a mixing of pyroclastic material from multiple eruptions from different volcanoes. Indeed, while rhyolites are typical of the early activity of Vico volcano, the foiditic composition is also unusual within the Latium volcanics being almost exclusive to the Colli Albani (e.g., Cross et al., 2014; Gaeta et al., 2016). Specifically, the age of SPF4 is within a relatively long interval of frequent explosive activity of the Colli Albani during which was emplaced the Centogocce fall succession (Giordano et al., 2006), dated to 405.3 ± 8 ka – 402.2 ± 5 ka (Karner et al., 2001, Gaeta et al., 2016, ages recalculated).

About the Vico component of SPF4, the age of 403.5 ± 4.2 ka (SC11 + P1C8) would be consistent with that of Vico γ, constrained between the ages of Vico δ (399.7 ± 3.0 ka, Fig. 5) and Vico β_{top} (406.4 ± 2.0 ka, Fig. 5). However, the glass composition does not support the correlation of SPF4 with Vico γ (Fig. 9c) and therefore we cannot propose any conclusive attribution. The p-value for SPF4 of Via della Pisana 1 (sample P1C8) also supports a mixing of at least two distinct eruptions products relatively close in age. Specifically, the bifurcation of the age probability diagram obtained for SPF4 at Via della Pisana 1, with a peak centred at ca. 405 ka and another at ca. 400 ka (Fig. 5), could approximate the ages of the two distinct eruptive events.

In summary, SPF4 is likely a volcaniclastic layer containing both Vico and Colli Albani eruption products, emplaced in a relatively short time-span of few millennia.

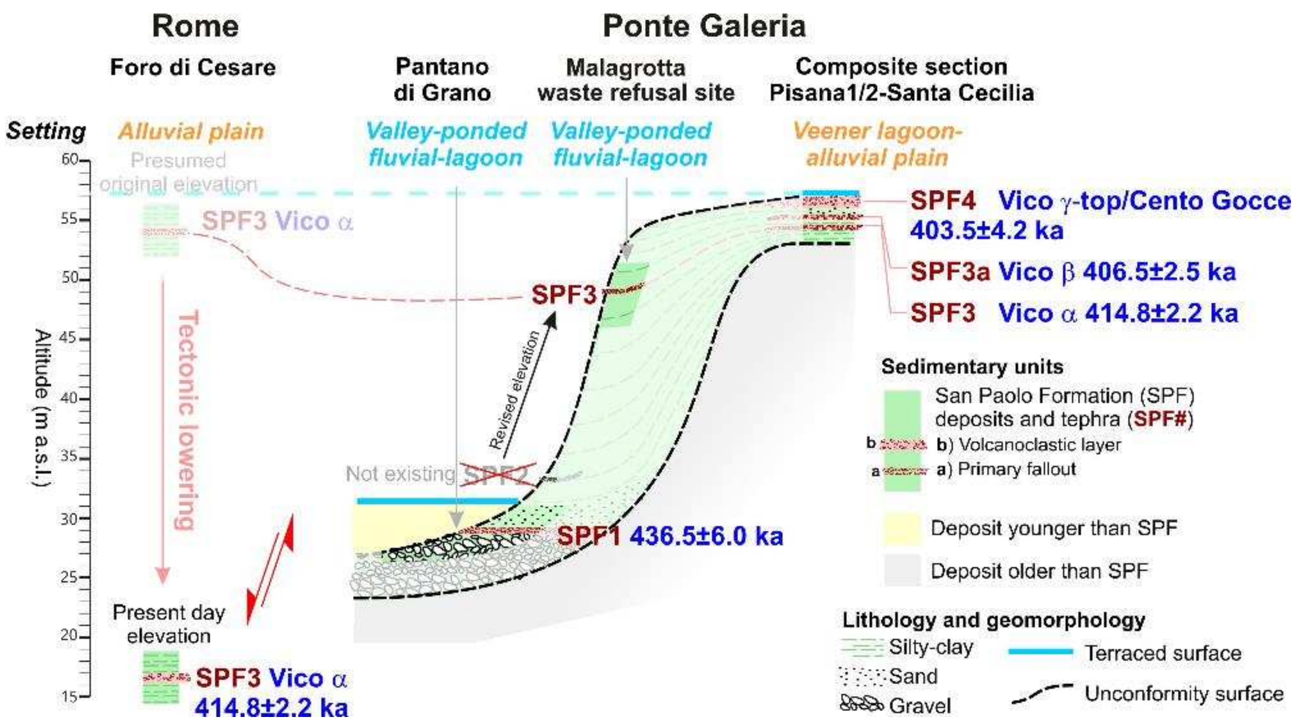

Figure 10. Summary of the sedimentary and geomorphological setting and tephrochronological framework of the MIS 12-MIS 11 aggradational succession of the San Paolo Formation.

5.3. Reappraising the central Mediterranean distal tephrostratigraphy of the MIS 11c period

5.3.1. General Framework

Several recent studies of distal tephrostratigraphic archives reported the occurrence of either Vico α or Vico β, as well as of other eruptive units spanning the MIS 11 period (e.g., Marcolini et al., 2003; Regattieri et al., 2016; Marra et al., 2016; Kousis et al., 2018; Leicher et al., 2016, 2019). However, due to the poor geochronological constraints and glass geochemical composition available for these pyroclastic units in proximal settings, the proposed correlations were unavoidably affected by a large uncertainty. The new data allow us a critical revision of the literature data and to assess the soundness of the previous interpretations.

5.3.2. Origin of Pre-Vico α and its identification in Fucino Basin and Lake Ohrid

Fucino Basin - In a recent paper, Giaccio et al. (2019) provided a first tephrochronological framework of a succession of ~130 tephra layers from a sediment core of the Fucino Basin (Central Italy), spanning the last 430 ka. The lowermost recognized tephra layer of this series labelled TF-126, was directly dated by $^{40}Ar/^{39}Ar$ method at 424.3 ± 3.2 ka and, based on the geochemical and chronological constraints available at that time, correlated to the Castel Broco eruption, from Vulsini Volcanic district. The age of this tephra is also consistent with the indirect chronological constraints now available for Pre-Vico α, which at Civita Castellana is framed by Vico α (414.5 ± 2.2 ka) and the TRSN (457.4 ± 2.0 ka) (Fig. 3). Notably, when comparing the composition of the glass from Pre-Vico α with both TF-126 and its potential equivalent Castel Broco, the Pre-Vico α eruption precisely matches TF-126 geochemistry (Fig. 11a). Therefore, assuming that the correlation between TF-126 and Castel Broco is reliable, this outstanding geochemical matching would point out that Pre-Vico α is not a Vico eruption, but a distal occurrence of the Vulsini eruption of Castel Broco. However, while the geochemical correlation between Pre-Vico α and TF-126 is unquestionable, some difference between the glass compositions of Pre-Vico α and Castel Broco can be noted (Fig. 11a). Nevertheless, the wider compositional spectrum of TF-126 covers both Pre-Vico α and Castel Broco, suggesting that both tephra are correlated with TF-126 but also that they likely are not representative of the entire composition variability of the eruption, because of the incomplete sampling (i.e., Castel Broco) and/or a geochemical zoning depending of geographical dispersion of the eruptive products (i.e., Pre-Vico α). Furthermore, also the relatively thin thickness and fine-grain size of Pre-Vico α is consistent with a mid-distal lithofacies, rather than a near-source lithology. We therefore interpret Pre-Vico α as a mid-distal occurrence of a Vulsini eruption, likely corresponding to Castel Broco.

Lake Ohrid - Another distal tephra, chronologically consistent with TF-126/Pre-Vico α/Castel Broco, is the layer OH-DP 1733 from the Lake Ohrid succession. The multiproxy paleoclimatic record of Lake Ohrid (Wagner et al., 2019), indicates that it occurs at the beginning of the MIS 11c interglacial with a modelled age of 423.9 ± 6.4 ka (Leicher et al., 2019), therefore very close to that of TF-126. However, as already shown in Giaccio et al. (2019) and supported by the new glass compositional data acquired for OH-DP 1733, it is geochemically incompatible with TF-126 (Fig. 11a). Specifically, the relatively high Cl content of OH-DP 1733 of 0.25 ± 0.05 wt% and its CaO/FeO ratio of 0.99 ± 0.17 are typical of the Roccamonfina volcanic centre products (Giaccio et al., 2019), and thus confirm the origin from this volcanic complex (Leicher et al., 2019).

5.3.3. Putative Vico eruptions in Sant'Abbondio section, Castel di Guido archaeological site, Lower Valdarno fluvial succession, Sulmona Basin and Lake Ohrid

Sant'Abbondio Section – The Sant'Abbondio section, located in the eastern sector of Vico and Sabatini volcanic areas (Fig. 1), consists of ~15 m thick sedimentary succession, including ten primary pyroclastic fall units separated by fluvial deposits and/or paleosols (Marra et al., 2014b). It is tephrochronologically constrained between the TRSN (453.4 ± 2.0 ka) and Magliano Romano Plinian Fall (313.0±2.0 ka) (Marra et al., 2014b), which occur at the bottom and top of the succession, respectively. Among the ten pyroclastic units of the Sant'Abbondio section, Marra et al. (2014) reported the occurrence of Vico α and Vico β, corresponding to the SA Fall 2 and SA Fall 3, respectively. By comparing the glass composition of SA Fall 2 and SA Fall 3 (Marra et al., 2014) with the geochemical dataset we got here for the proximal Vico α and Vico β units, we can surely confirm the attribution of SA Fall 2 to Vico α. However, the correlation of the SA Fall 3 with Vico β is clearly not supported (Fig. 11c). On the other hand, the composition of SA Fall 3 matches that of the CC2 pumice fallout, likely from an unknown Sabatini eruption, directly lying on Vico a Plinian deposits at Civita Castellana section (Fig. 11c).

Castel di Guido archaeological site – The chronology of this Lower Palaeolithic site (Radmilli and Boschian, 1996), belonging to the rich complex of the Middle Pleistocene archaeological and paleontological sites of the Roman Province (Fig. 1; Boschian et al., 2010), was recently revised by Marra et al. (2018). Specifically, based on the peculiar rhyolitic composition of a sub-primary pumice layer (CDG-S1) correlated to Vico α, the authors ascribed the site to the MIS 11 San Paolo Formation, thus changing the previous chronological attribution to the MIS 9 period. Though this has no impact on the chronological attribution of the Castel di Guido site to the MIS 11, the glass composition of the CDG-S1 tephra does not support a univocal correlation with Vico α, as it composition is consistent with both Vico α and Vico β (Fig. 11b).

Lower Valdarno –The Middle Pleistocene fluvial deposits of the Lower Valdarno valley, along the Arno River (Tuscany, central Italy), contain one tephra layer that was attributed to the Vico volcano (named Collesalvetti in Biagazzi et al., 1994 and Montopoli in Marcolini et al., 2003) no precise correlation for this tephra has been until now proposed. This tephra is stratigraphically recorded above a pedogenic horizon (Campani Quarry paleosol) rich in temperate mollusc and small mammal fossils attributed to the MIS 11 (Marcolini et al., 2003). It was dated by fission track dating method on apatite to 460 ± 50 ka (uncertainties at 1σ, Biagazzi et al., 2000), and has a glass composition, determined by EDS analyses, ranging from trachyte to rhyolite (Biagazzi et al., 1994).

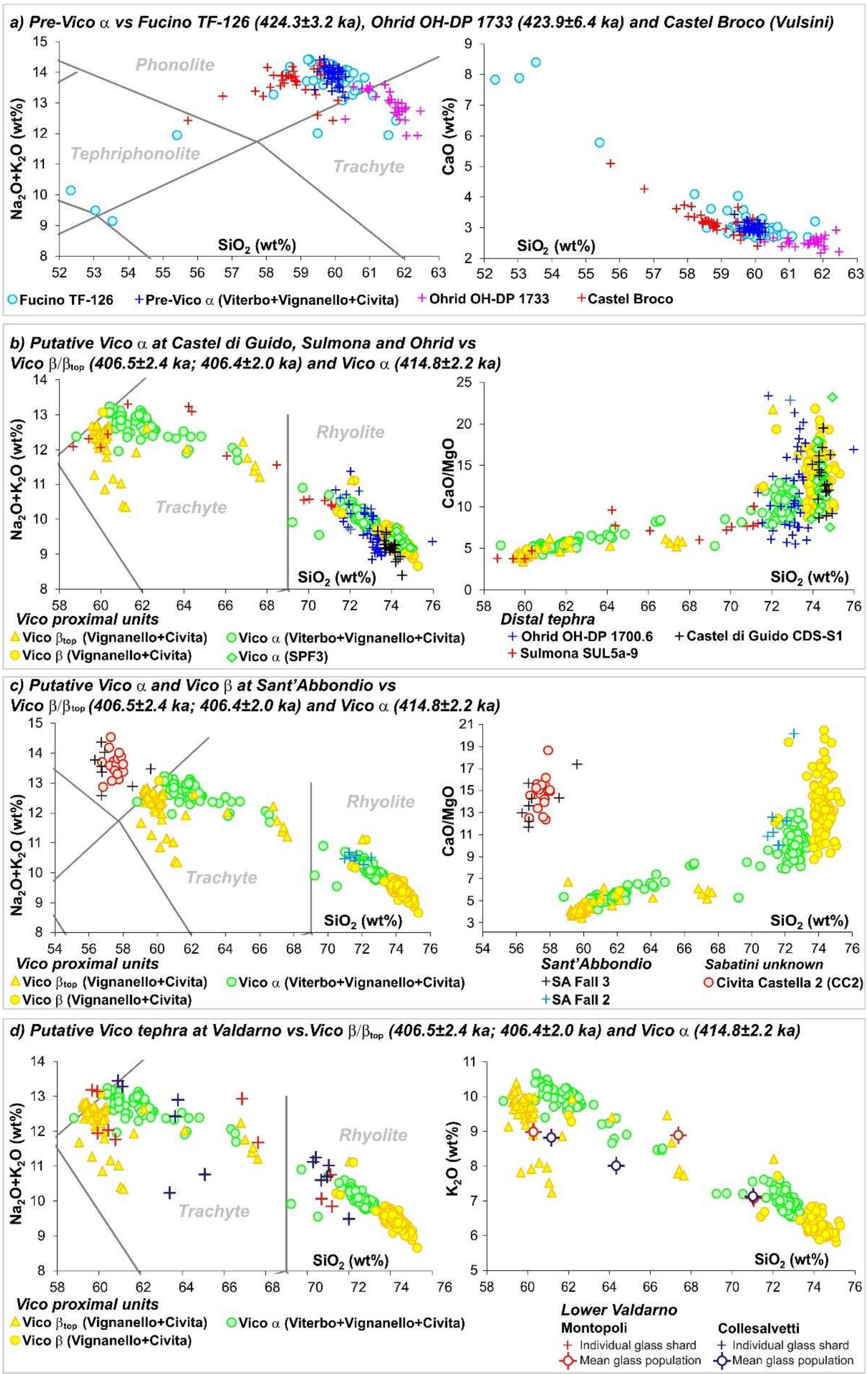

Figure 11. Total alkali versus silica classification diagram (Le Maitre, 2002) and representative bi-plots of the glass composition of distal tephra previously attributed the early Vico explosive activity compared with the glass composition from the proximal Vico α and Vico β units. **a)** Comparison of pre-Vico α with Fucino TF-126, Ohrid OH-DP 1733 and Castel Broco. **b)** Comparison of the Sulmona tephra

SUL5a-9 and Ohrid OH-DP 1700.3 with the Vico α and Vico β proximal units. **c)** Comparison of SA Fall 2 and SA Fall 3 from Sant'Abbondio section with the proximal units Vico α and Vico β and with the CC2 pumice fall from Civita Castellana section. **d)** Comparison of the Lower Valdarno tephra with the Vico α and Vico β proximal units. Data source: glass-WDS and $^{40}Ar/^{39}Ar$ of TF-126 and glass-WDS of Castel Broco: Giaccio et al (2019); glass-WDS of Castel di Guido – S1: Marra et al. (2018); glass-WDS of OH-DP 1733: Leicher et al. (2019) and this study; glass-WDS of SUL5a-9: Regattieri et al. (2016); glass-WDS of OH-DP 1700.6: Kousis et al. (2018); glass-EDS Lower Valdarno tephra: Biagazzi et al. (1994).

The comparison with our improved geochemical and geochronological dataset confirms the attribution of this tephra to the early Vico activity, but a definitive correlation with either Vico α or Vico β is currently quite hard to propose. In fact, in TAS diagram, while the trachyte component of Montopoli tephra is similar to that of Vico β, that of Collesalvetti is more similar to the trachyte component of Vico α (Fig. 11d). Using other bivariate diagrams (e.g., SiO_2 vs K_2O) makes the discrimination even more uncertain (Fig. 11d).

In conclusion, we are inclined to consider that the EDS data collected for this Lower Valdarno tephra are both insufficient in number and are lacking the accuracy and precision required for reliably discriminating between Vico α or Vico β, so making a definitive correlation uncertain. In spite of this remaining uncertainty, regardless of the precise attribution of the Valdarno tephra to Vico α or Vico β, our new data confirm the attribution of the Campani Quarry paleosol, and of its faunal assemblage, to the MIS 11, and precisely to the early part of the MIS 11c interglacial, surely older than ca. 406 ka.

Sulmona Basin - A trachyte-rhyolite tephra (SUL5a-9) has been reported in the MIS 12-MIS 11 interval of the lacustrine succession of Sulmona Basin (central Italy) (Regattieri et al., 2016). According to the oxygen isotope palaeohydrological record of Sulmona, SUL5a-9 occurs in the early stage of the MIS 11c interglacial (ca. 425-395 ka) and was correlated to Vico α (Regattieri et al., 2016). In the light of the present wider reference compositional dataset for both Vico α and Vico β, the correlation of SUL5a-9 to Vico α remains controversial (Fig. 11b). Indeed, even if the rhyolitic component of SUL5a-9 would seem more compatible with Vico α, the trachyte one appears more similar to that of Vico β_{top}. Thus, at present, a definitive attribution of SUL5a-9 to either Vico α or Vico β_{top} is hardly tenable.

Lake Ohrid – A K-rhyolitic cryptotephra (OH-DP 1700.6) has been recognised by Kousis et al. (2018) in the MIS 11 high-resolution pollen record from Lake Ohrid. Based on its position within the MIS 11c interglacial (modelled age 414.8 ± 3.2 ka; Leicher et al., 2019), its peculiar K-rhyolitic composition, and the few geochemical data available for the near-source sections, Kousis et al. (2018) tentatively correlated OH-DP 1700.6 to the rhyolitic pumice layer C7 (SPF3, Figs. 2, 6 and 9, San Paolo Formation) dated to 413.5 ± 2.0 ka (Karner et al., 2001a) and attributed to Vico α (Marra et al., 2014). Our new reference geochemical dataset for the early Vico activity confirms the attribution of OH-

DP1700.6 to Vico α. Indeed, though more scattered, the rhyolitic glass composition of OH-DP 1700.6 appears more similar to the rhyolitic component of Vico α rather than that of Vico β (Fig. 11b). Nevertheless, Kousis et al. (2018) correlated OH-DP 1700.6 to Vico β instead of Vico α. However, we now know that they used data from the Roman tephra that are equivalent to Vico α, thus the attribution to Vico β was a mere terminological misunderstanding, due to the lack of clarity in the nomenclature of the Vico tephra occurring in the Roman, which persisted and mislead scholars until the present study.

5.3.4. Timing of Vico Period I activity and geographical dispersion its products

The new chronological constraints obtained for Vico Period I and the proximal-distal correlations discussed in the previous section, allow us to precisely define the timing of explosive activity and the geographical dispersal of each individual eruptive units as briefly summarised in the following. The earliest activity of Vico volcano took place at 414.8 ± 2.2. ka with the Plinian eruption of Vico α. This is the most widespread units of the Vico Period I, as testified by its recognition in the ultra-distal setting of Ohrid lake and in other possible localities of the central Italy area (Fig. 12). After an inter-eruptive quiescence of 8.3 ± 3.2 kyrs, the second Plinian eruption of Vico β occurred at 406.5 ± 2.4 ka. This is likely the second largest explosive event of Vico Period I with a dispersal area likely including a wide portion of the central Italy (Fig. 12), though, as discussed above, in some localities distinguishing between Vico α and Vico β is currently prevented by the low quality of the available geochemical data. Vico β eruption was immediately followed by the Vico β_{top} eruption, dated at 406.4 ± 2.0, i.e., an age statically indistinguishable from that of Vico β. This suggest that Vico β was likely multiple events separated by a very short temporal break, not resolvable by the $^{40}Ar/^{39}Ar$ geochronology. Unfortunately, no $^{40}Ar/^{39}Ar$ was acquired for the fourth eruption of Vico γ, so preventing an estimation of the inter-eruptive interval elapsed since Vico β/β_{top} eruption(s). On the other hand, the age we got for Vico δ at 399.7 ± 3.2 ka indicates that a millennial-long interval separates the Vico β/β_{top} eruptions to this most recent event of the Vico Period I. So far, no distal occurrence of Vico γ and Vico δ has been recognised.

6. CONCLUDING REMARKS AND PERSPECTIVES

In this paper we have stratigraphically, chronologically and geochemically characterized the until now poorly constrained early explosive activity of Vico volcano, including the main Vico α and Vico β

Plinian eruptions and minor events, greatly improving the tephrochronological framework for the MIS 11c interglacial (~425-395 ka) of the central Mediterranean area. This allowed us to trace these units along an ideal NW-SE trending transect linking the Vico volcano to the Roman MIS 11 aggradational succession (SPF), where we substantially refine the chronology. Moreover, these new data allowed us to reappraise some putative identifications of the Vico tephra in intermediate (i.e., Castel di Guido, Sant'Abbondio), distal (Fucino, Sulmona, Valdarno) and ultra-distal (Ohrid) settings, which were previously suggested on the basis of the poor chronological and/or geochemical data. A synthesis of the tephra correlations of the proximal, mid and distal sedimentary successions, either investigated for the first time in this study or revised from literature, is shown in Figure 12. Specifically, while we have confirmed the identification of Vico α in Lake Ohrid succession, the putative identification of Vico α in the sedimentary successions of Sulmona Basin (central Italy), Valdarno (Tuscany, central Italy) and of the Roman archaeological site of Castel di Guido, remained unresolved. Indeed, the Vico tephra found in these three localities are geochemically consistent with either Vico α or Vico β Plinian eruptions. As a general observation, we notice that for most of these revised occurrences of the Vico tephra, a wider, statistically significant, geochemical compositional dataset, acquired via accurate and precise WDS analyses, would be needed to definitively attribute them to either Vico α or Vico β. Furthermore, laser ablation trace element glass compositions of both proximal and distal Vico tephra likely would further help in discriminating these two Vico Plinian eruptions. Future acquisitions of such data are thus pivotal for setting robust discriminating criteria.

Future developments of the ongoing tephrochronological and palaeoclimatic multi-proxy investigations of the regional late MIS 12-MIS 11 successions (e.g., the Fucino and Sulmona lacustrine records, the Roman archaeological and aggradational successions) are likely to benefit greatly from the presented geochronological and geochemical data. Indeed, thorough tephra geochemical fingerprinting, the high precision $^{40}Ar/^{39}Ar$ dating presented in this study can be propagated on a regional and extra-regional scale, allowing paleoclimatic, archaeological, sea-level change records, and/or of any other kind of proxy series and sedimentary successions where Vico tephra will be found, to be precisely dated. In particular, this will give us the unique opportunity of reliably synchronizing, via tephra correlations, the central Italy paleoenvironmental archives with the Roman records of the sea-level rise during the late MIS 12-MIS 11c interval, and thus of comparing and evaluating the dynamics of the processes that acted in the two systems in a robust and coherent chronological framework.

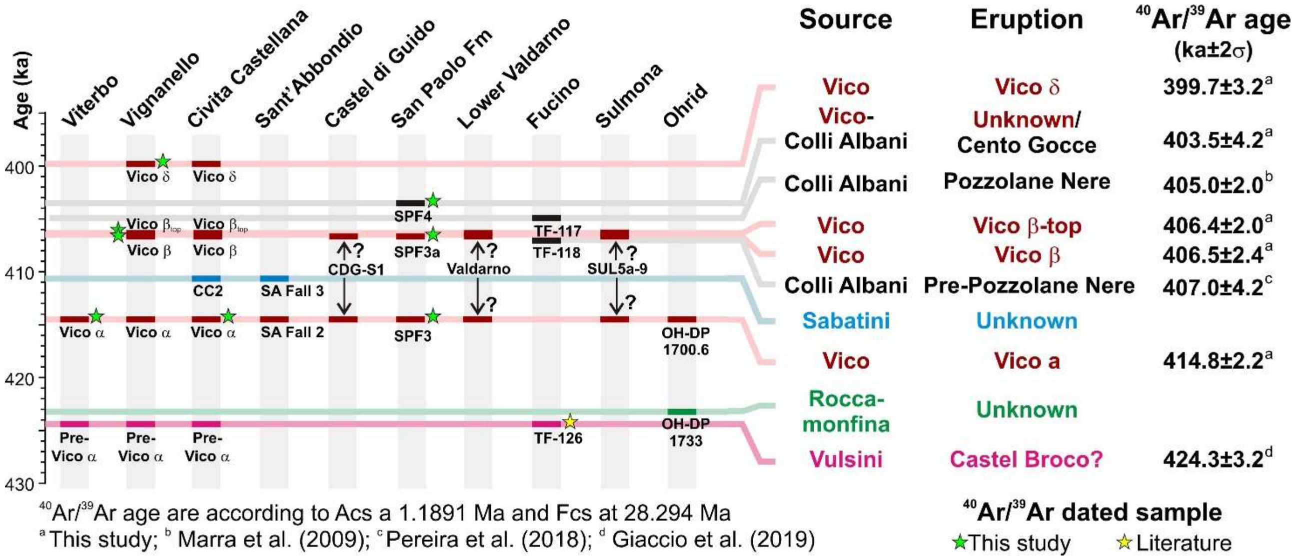

Figure 12. Summary of the tephra correlations among the proximal, intermediate and distal successions, either investigated in this study or revised from literature.

ACKNOWLEDGEMENTS

Field work and the acquisition of the major element composition was supported by the project "FUcino Tephrochronology Unites Quaternary REcords (FUTURE)", financed by the Italian Ministry of Education, University and Research (MIUR, grant PRIN No. 20177TKBXZ_003).

REFERENCES

Albert, P., Giaccio, B., Isaia, R., Costa, A., Niespolo, E.M., Nomade, S., Pereira, A., Renne, P.R., Hinchliffes, A., Mark, D.F., Brown, R.J., Smith, V.C., 2019. Evidence for a large-magnitude eruption from Campi Flegrei caldera (Italy) at 29 ka. Geology. https://doi.org/10.1130/G45805.1

Amato, V., Aucelli, P.P.C., Cesarano, M., Filocamo, F., Leone, N., Petrosino, P., Rosskopf, C.M., Valente, E., Casciello, E., Giralt, S., Jicha, B.R., 2018. Geomorphic response to late Quaternary tectonics in the axial portion of the Southern Apennines (Italy): a case study from the Calore River valley. Earth Surf. Process. Landforms 43, 2463–2480.

Barberi, F., Buonasorte, G., Cioni, R., Fiordelisi, A., Foresi, L., Iaccarino, S., Laurenzi, M.A., Sbrana, A., Vernia, L., Villa, I.M, 1994. Plio-Pleistocene geological evolution of the geothermal area of Tuscany and Latium. Mem. descr. della Carta Geol. d'It 49, 77-134.

Bigazzi, G., Bonadonna. F.P., Cioni, R., Leone, G., Sbrana, A., Zanchetta, G. 1994. Nuovi dati geochimici, petrografici e geocronologici su alcune cineriti plio-pleistoceniche del Lazio e della Toscana. Memorie Descrittive della Carta Geologica d'Italia 49, 135–150.

Bigazzi G, Zanchetta G, Bonadonna FP, Leone G. 2000. Nuovi dati cronologici sui depositi cineritici del Valdarno inferiore (Toscana). Bollettino della Societa` Geologica Italiana 119: 121–124.

Boschian, G., Sacc_a, D., 2010. Ambiguities in human and elephant interactions? Stories of bones, sand and water from Castel di Guido (Italy). Quat. Int. 214, 3-16.

Bourne, A.J., Albert, P.G., Matthews, I.P., Trincardi, F., Wulf, S., Asioli, A., Blockley, S.P.E., Keller, J., Lowe, J.J., 2015. Tephrochronology of core PRAD 1-2 from the Adriatic Sea: insights into Italian explosive volcanism for the period 200-80 ka. Quat. Sci. Rev. 116, 28-43.

Bowen, D.Q., 2010. Sea level~400 000 years ago (MIS 11): analogue for present and future sea-level? Clim. Past, 6, 19–29.

Cioni, R., 1993. Il Complesso di Bolsena e il vulcanismo alcalino-potassico del Lazio settentrionale. Unpublished PhD Dissertation, Dipartimento di Scienze della Terra, Università degli Studi di Pisa, 236 pp.

Cioni, R., Sbrana, A., Bertagnini, A., Buonasorte, G., Landi, P., Rossi, U., Salvati, L., 1987. Tephrostratigraphic correlations in the Vulsini, Vico and Sabatini volcanic successions. Periodico di Mineralogia 56 (2-3), 137-155.

Costa, A., Folch, A., Macedonio, G., Giaccio, B., Isaia, R., Smith, V.C., 2012. Quantifying volcanic ash dispersal and impact of the Campanian Ignimbrite super-eruption. GEOPHYSICAL RESEARCH LETTERS, VOL. 39, L10310, doi:10.1029/2012GL051605

Cross, J., Tomlinson, E., Giordano, G., Smith, V.C., De Benedetti, A., Robergue, J., Manning, C., Wulf, S., Menzies, M., 2014. High level triggers for explosive mafic volcanism: Albano Maar, Italy, Lithos, 190-191, 137-153

Dutton, A., Carlson, A., Milne, G., Long, A.J., Clark, P.U., DeConto, R., Horton, B.P., Rahmstorf, S., Raymo, M.E., 2015, Sea-level rise due to polar ice-sheet mass loss during past warm periods, Science, vol. 349, no. 6244, doi: 10.1126/science.aaa4019

Flisch, M. 1982. « Potassium-Argon Analysis », Odin, G. S. (Ed.), Numerical Dating in Stratigraphy, John Wiley & Sons, New York, 151-158.

Gaeta, M., Freda, C., Marra, F., Arienzo, I., Gozzi, F., Jicha, B., Di Rocco, T., 2016. Paleozoic metasomatism at the origin of Mediterranean ultrapotassic magmas: constraints from time-dependent geochemistry of Colli Albani volcanic products (Central Italy). Lithos 244, 151-164. doi:10.1016/j.lithos.2015.11.034

Giaccio, B., Castorina, F., Nomade, S., Scardia, G., Voltaggio, M., Sagnotti, L., 2013. Revised Chronology of the Sulmona Lacustrine Succession, Central Italy. Journal of Quaternary Science 28, 545–551. doi:10.1002/jqs.2647

Giaccio, B., Galli, P., Peronace, E., Arienzo, I., Nomade, S., Cavinato, G.P., Mancini, M., Messina, P., Sottili, G., 2014. A 560-440 ka tephra record from the Mercure Basin, southern Italy: volcanological and tephrostratigraphic implications. Journal of Quaternary Science 29, 232–248. doi:10.1002/jqs.2696

Giaccio, B., Regattieri, E., Zanchetta, G., Nomade, S., Renne, P.R., Sprain, C.J., Drysdale, R.N., Tzedakis, P.C., Messina, P., Scardia, G., Sposato, A., Bassinot, F., 2015. Duration and dynamics of the best orbital analogue to the present interglacial. Geology 43, 603–606.

Giaccio, B., Niespolo, E.,Pereira A., Nomade, S., Renne, P.R., Albert, P.G., Arienzo, I., Regattieri, E., Wagner, B., Zanchetta, G., Gaeta, M., Galli, P., Mannella, G., Peronace, E., Sottili, G., Florindo, F., Leicher, N., Marra, F., Tomlinson, E.L., 2017. First integrated tephrochronological record for the last ~190 kyr from the Fucino Quaternary lacustrine succession, central Italy. Quaternary Science Reviews 158, 211-234.

Giaccio, B., Leicher, N., Mannella, G., Monaco, L., Regattieri, E., Wagner, B., Zanchetta, G., Gaeta, M., Marra, F., Nomade, S., Palladino, D.M., Pereira, A., Scheidt, S., Sottili, G., Wonik, T., Wulf, S., Zeeden, C., Ariztegui, D., Cavinato, G.P., Dean, J.R., Florindo, F., Leng, M.J., Macrì, P., Niespolo, E.M., Renne, P.R., Rolf, C., Sadori, L., Thomas, C., Tzedakis, P.C., 2019. Extending the tephra and palaeoenvironmental record of the Central Mediterranean back to 430 ka: A new core from Fucino Basin, central Italy. Quaternary Science Reviews, 225, 106003.

Giordano, G., De Benedetti, A.A., Diana, A., Diano, G., Gaudioso, F., Marasco, F., Miceli, M., Mollo, S., Cas, R.A.F., Funiciello, R., 2006. The Colli Albani mafic caldera (Roma, Italy): Stratigraphy, structure and petrology. Journal of Volcanology and Geothermal Research 155, 49–80. doi: 10.1016/j.jvolgeores.2006.02.009

Guillou H, Scao V., Nomade S., 2018. 40Ar/39Ar age of cryptochron C2r.2r-1 as recorded in a lava sequence within the Ko'olau volcano (Hawaii, USA). Quaternary Geochronology 43,91–101. doi : 10.1016/j.quageo.2017.10.005

Grant, K.M., Rohling, E.J., Ramsey, C.B., Cheng, H., Edwards, R.L., Florindo, F., Heslop, D., Marra, F., Roberts, A.P., Tamisiea, M.E., Williams, F., 2014. Sea-level variability over five glacial cycles. Nature communications 5, doi:10.1038/ncomms6076

Insinga, D.D., Tamburrino, S., Lirer, F., Vezzoli, L., Barra, M., De Lange, G.J., Tiepolo, M., Vallefuoco, M., Mazzola, S., Sprovieri, M., 2014. Tephrochronology of the astronomically-tuned KC01B deep-sea core, Ionian Sea: insights into the explosive activity of the Central Mediterranean area during the last 200 ka. Quat. Sci. Rev. 85, 63-84.

Karner, D.B., Marra, F., 1998. Correlation of fluviodeltaic aggradational sections with glacial climate history: A revision of the Pleistocene stratigraphy of Rome. Geological Society of America Bulletin 110, 748–758.

Karner, D.B., Marra, F., 2003. 40Ar/39Ar dating of Glacial Termination V and duration of the Stage 11 highstand, in: Earth's Climate and Orbital Eccentricity: The Marine Isotope Stage 11 Question, American Geophysical Union, Geophysical Monograph, 137, 61-66.

Karner, D.B., Renne, P.R., 1998. 40Ar/39Ar geochronology of Roman volcanic province tephra in the Tiber River valley: Age calibration of middle Pleistocene sea-level changes. Geological Society of America Bulletin 110, 740-747.

Karner, D.B., Marra, F., Renne, P.R., 2001. The history of the Monti Sabatini and Alban Hills volcanoes: groundwork for assessing volcanic-tectonic hazards for Rome. Journal of Volcanology and Geothermal Research, 107, 185-219.

Kousis, I., Koutsodendris, A., Peyron, O., Leicher, N., Francke, A., Wagner, B., Giaccio, B., Knipping, M., Pross, J., 2019. Centennial-scale vegetation dynamics and climate variability in SE Europe during Marine Isotope Stage 11 based on a pollen record from Lake Ohrid. Quat. Sci. Rev. 190, 20–38.

Kuiper K. F., Deino A., Hilgen F. J., Krijgsman W., Renne P. R. and Wijbrans J. R. 2008. Synchronizing the rock clocks of Earth history. Science 320, 500–504.

Laurenzi, M.A., Villa, I.M., 1987. ^{40}Ar/^{39}Ar chronostrastigraphy of Vico ignimbrites: Periodico di Mineralogia, v. 56, p. 285-293.

Lee, J.Y., Marti, K., Severinghaus, J.P., Kawamura, K., Hee-Soo, Y., Lee, J.B., Kim, J.S., 2006. A redetermination of the isotopic abundances of atmospheric Ar. Geochimica et Cosmochimica Acta 70, 4507-4512. doi: 10.1016/j.gca.2006.06.1563

Leicher, N., Zanchetta, G., Sulpizio, R., Giaccio, B., Wagner, B., Nomade, S., Francke, A., et Del Carlo, P., 2016. First tephrostratigraphic results of the DEEP site record from Lake Ohrid (Macedonia and Albania). Biogeosciences 13, 2151–2178. doi:10.5194/bg-13-2151-2016

Leicher, N., Giaccio, B., Zanchetta, G., Wagner, B., Francke, A., Palladino, D.M., Sulpizio, R., Albert, P.G., Tomlinson, E.L. 2019. Central Mediterranean explosive volcanism and tephrochronology during the last 630 ka based on the sediment record from Lake Ohrid. Quaternary Science Reviews 226, 106021

Le Maitre, R. W., 2002. Igneous rocks a Classification and Glossary of Terms Recommendations of the International Union of Geological Sciences, Sub-Commission on the Systematics of Igneous Rocks, Cambridge University Press, 236 p. http://dx.doi.org/10.1017/CBO978051153558

Locardi, E., Funiciello, R., Lombardi, G., Parotto, M., 1977. The main volcanic groups of Latium (Italy): relations between structural evolution and petrogenesis. Geol. Rom 15:279-300

Mannella, G., Giaccio, B., Zanchetta, G., Regattieri, E., Niespolo, E., Pereira, A., Renne, P.R., Nomade, S., Leicher, N., Perchiazzi, N., Wagner, B., 2019. Palaeoenvironmental and palaeohydrological variability of mountain areas in the central Mediterranean region: A 190 ka-long chronicle from the independently dated Fucino palaeolake record (central Italy). Quaternary Science reviews 210, 190-210.

Mannella, G., Giaccio, B., Zanchetta, G., Regattieri, E., Niespolo, E., Pereira, A., Renne, P.R., Nomade, S., Leicher, N., Perchiazzi, N., Wagner, B., 2019. Palaeoenvironmental and palaeohydrological variability of mountain areas in the central Mediterranean region: A 190 ka-long chronicle from the independently dated Fucino palaeolake record (central Italy). Quaternary Science reviews 210, 190-210.

Marra, F., Florindo, F., Karner, D.B., 1998. Paleomagnetism and geochronology of early Middle Pleistocene depositional sequences near Rome: comparison with the deep sea δ18O climate record. Earth Planet. Sci. Lett. 159, 147-164.

Marra, F., Florindo, F., Boschi, E., 2008. History of glacial terminations from the Tiber River, Rome: Insights into glacial forcing mechanisms. Paleoceanography 23, 1-17. doi:10.1029/2007PA001543

Marra, F., Pandolfi, L., Petronio, C., Di Stefano, G., Gaeta, M., Salari, L., 2014a. Reassessing the sedimentary deposits and vertebrate assemblages from Ponte Galeria area (Rome, central Italy): An archive for the Middle Pleistocene faunas of Europe. Earth-Science Reviews 139, 104-122. doi: 10.1016/j.earscirev.2014.08.014

Marra, F., Sottili, G., Gaeta, M., Giaccio, B., Jicha, B., Masotta, M., Palladino, D.M., Deocampo, D., 2014b. Major explosive activity in the Sabatini Volcanic District (central Italy) over the 800-390 ka interval: geochronological - geochemical overview and tephrostratigraphic implications. Quaternary Science Reviews 94, 74-101. doi:10.1016/j.quascirev.2014.04.010

Marra, F., Ceruleo, P., Jicha, B., Pandolfi, L., Petronio, C., Salari, L., 2015. A new age within MIS 7 for the Homo neanderthalensis of Saccopastore in the glacio-eustatically forced sedimentary successions of the Aniene River Valley, Rome. Quaternary Science Reviews 129, 260-274. http://dx.doi.org/10.1016/j.quascirev.2015.10.027

Marra, F., Rohling, E.J., Florindo, F., Jicha, B., Nomade, S., Pereira, A., Renne, P.R., 2016. Independent 40Ar/39Ar and 14C age constraints on the last five glacial terminations from the aggradational successions of the Tiber River, Rome (Italy). Earth Planet Sci. Lett. 449, 105-117. http://dx.doi.org/10.1016/j.epsl.2016.05.037

Marra, F., Jicha, B., Florindo, F., 2017a. 40Ar/39Ar dating of Glacial Termination VI: constraints to the duration of Marine Isotopic Stage 13. Scientific Reports 7: 8908. DOI:10.1038/s41598-017-08614-6

Marra, F., Ceruleo, P., Pandolfi, L., Petronio, C, Rolfo, M.F., Salari, L., 2017b. The Aggradational Successions of the Aniene River Valley in Rome: Age Constraints to Early Neanderthal Presence in Europe. PLoS ONE 12(1): e0170434. doi:10.1371/journal.pone.0170434

Marra, F., Castellano, C., Cucci, L, Florindo, F., Gaeta, M., Jicha, B., Palladino, D.M., Sottili, G., Tertulliani, A., Tolomei, C., 2020. Monti Sabatini and Colli Albani: the dormant twin volcanoes at the gates of Rome, Scientific Reports, in press.

Marra; F., Rosa, C. 1995. Stratigrafia e assetto geologico dell’area romana. Mem. Descr. Della carta Geol. D’Italia 50, 49-118.

Masson-Delmotte, V., Stenni, B., Pol, K., Braconnot, P., Cattani, O., Falourd, S., Kageyama, M., Jouzel, J., Landais, a., Minster, B., Barnola, J.M., Chappellaz, J., Krinner, G., Johnsen, S., R€othlisberger, R., Hansen, J., Mikolajewicz, U., Otto- Bliesner, B., 2010. EPICA Dome C record of glacial and interglacial intensities. Quat. Sci. Rev. 29, 113-128.

Milli, S., 1997. Depositional setting and high-frequency sequence stratigraphy of the middle-upper Pleistocene to Holocene deposits of the Roman basin. Geologica Romana 33, 99-136.

Niespolo, E.M., Rutte, D., Deino, A. et Renne, P.R., 2017. Intercalibration and age of the Alder Creek sanidine 40Ar/39Ar standard. Quaternary Geochronology in press. http://dx.doi. org/10.1016/j.quageo.2016.09.004

Nomade, S., Gauthier, A., Guillou, H., Pastre, J.F., 2010. 40Ar/39Ar temporal framework for the Alleret maar lacustrine sequence (French Massif-Central): Volcanological and paleoclimatic implications. Quaternary Geochronology 5, 20-27.

Paterne, M., Guichard, F., Duplessy, J.C., Siani, G., Sulpizio, R., Labeyrie, J., 2008. A 90,000-200,000 yrs marine tephra record of Italian volcanic activity in the Central Mediterranean Sea. J. Volcanol. Geotherm. Res. 177, 187-196.

Peccerillo, A., 2017. Cenozoic Volcanism in the Tyrrhenian Sea Region. DOI: 10.1007/978-3-319-42491-0

Pereira, A., Nomade, S., Voinchet, P., Bahain, J.J., Falguères, C., Garon, H., Lefèvre, D., Raynal, J.P., Scao, V., Piperno, M., 2015. The earliest securely dated hominin fossil in Italy and evidence of Acheulian occupation during glacial MIS 16 at Notarchirico (Venosa, Basilicata, Italy). Journal of Quaternary Science. doi : 10.1002/jqs.2809

Pereira, A., Nomade, S., Moncel, M.H., Voinchet, P., Bahain, J.J., Biddittu, I., Falguères, C., Giaccio, B., Manzi, G., Parenti, F., Scardia, G., Scao, V., Sottili, G., Vietti, A. Geochronological evidences of a MIS 11 to MIS 10 age for several key Acheulian sites from the Frosinone province (Latium, Italy): Archaeological implications. Quaternary Science Reviews 187, 112-129.

Peretto, C., Arnaud, J., Moggi-Cecchi, J., Manzi, G., Nomade, S., Pereira, A., Falguères, C., Bahain, J.J., Grimaud-Hervé, D., Berto, C., Sala, B., Lembo, G., Muttillo, B., Gallotti, G., Thun Hohenstein, U., Vaccaro, C., Coltorti, M., Arzarello, M., 2015. A Human Deciduous Tooth and New 40Ar/39Ar Dating Results from the Middle Pleistocene Archaeological Site of Isernia La Pineta, Southern Italy. PLoS ONE 10(10): e0140091. doi:10.1371/journal.pone.0140091

Perini, G., Francalanci, L., Davidson, J.P., Conticelli, S., 2004, Evolution and genesis of magmas from Vico volcano, Central Italy: multiple differentiation pathways and variable parental magmas: Journal of Petrology, v. 45, p. 139–182.

Petrosino, P., Jicha, B.R., Mazzeo, F.C., Russo Ermolli, E., 2014. A high resolution tephrochronological record of MIS 14–12 in the Southern Apennines (Acerno Basin, Italy). Journal of Volcanology and Geothermal Research 274, 34–50. doi:10.1016/j.jvolgeores.2014.01.014

Radmilli, A.M., Boschian, G., 1996. Storia della scoperta e degli scavi. In: Radmilli, A.M., Boschian, G. (Eds.), Gli scavi a Castel di Guido. Il più antico giacimento di cacciatori del Paleolitico inferiore nell'Agro Romano. Istituto Italiano di Preistoria e Protostoria, Firenze, 19-29.

Regattieri, E., Zanchetta, G., Drysdale, R.N., Isola, I., Hellstrom, J.C., Roncioni, A., 2014. A continuous stable isotope record from the penultimate glacial maximum to the Last Interglacial (159e121 ka) from Tana Che Urla Cave (Apuan Alps, central Italy). Quat. Res. 82 (2), 450-461.

Regattieri, E., Giaccio, B., Galli, P., Nomade, S., Peronace, E., Messina, P., Sposato, A., Boschi, C., Gemelli, M., 2016. A multi-proxy record of MIS 11–12 deglaciation and glacial MIS 12 instability from the Sulmona basin (central Italy). Quaternary Science Reviews 132, 129–145. doi:10.1016/j.quascirev.2015.11.015

Regattieri, E. Zanchetta, G., Isola, I., Zanella, E., Drysdale, R., Hellstrom, J.C., Zerboni, A., Dallai, J., Tema, E., Lanci, L., Costa, E., Magrì, F. 2019. Holocene Critical Zone dynamics in an Alpine catchment inferred from a speleothem multiproxy record: disentangling climate and human influences. Scientific Reports, DOI: 10.1038/s41598-019-53583-7.

Reimer, P.J., Bard, E., Bayliss, A., Beck, J.W., Blackwell, P.G., Bronk Ramsey, C., Buck, C.E., Cheng, H., Edwards, R.L., Friedrich, M., Grootes, P.M., Guilderson, T.P., Haflidason, H., Hajdas, I., Hatté, C., Heato, T.J., Hoffmann, D.L., Hogg, A.G., Hughen, K.A., Kaiser, K.F., Kromer, B., Manning, S.W., Niu, M., Reimer, R.W., Richards, D.A., Scott, E.M., Southon, J.R., Staff, R.A., Turney, C.S.M., van der Plicht, J. 2013. INTCAL13 and MARINE13 radiocarbon age calibration curves 0–50,000 years CAL BP. Radiocarbon, Vol 55 (4), 1869–1887.

Renne, P.R., Mundil, L.R., Balco, G., Min, K. et Ludwig, K.R., 2011. Joint determination of 40K decay constants and 40Ar*/40K for the Fish Canyon sanidine standard, and improved accuracy for 40Ar/39Ar geochronology. Response to the comment by W.H. Schwarz et al. Geochimica Cosmochimica Acta 75, 5097-5100.

Renne, P.R., Sprain, C.J., Richards, M.A., Self, S., Vanderkluysen, L., Pande, K., 2015. State shift in Deccan volcanism at the Cretaceous-Paleogene boundary, possibly induced by impact. Science 350, 76-78.

Rohling, E.J., Foster, G.L., Grant, K.M., Marino, G., Roberts, A.P., Tamisiea, M.E., Williams, F., 2014. Sea-level and deep-sea-temperature variability over the past 5.3 million years. Nature 508, 477-482.

Sadori, L., Koutsodendris, A., Panagiotopoulos, K., Masi, A., Bertini, A., Combourieu-Nebout, N., Francke, A., Kouli, K., Joannin, S., Mercuri, A.M., Peyron, O., Torri, P., Wagner, B., Zanchetta, G., Sinopoli, G., et Donders, T.H., 2016. Pollen-based paleoenvironmental and paleoclimatic change at Lake Ohrid (south-eastern Europe) during the past 500 ka. Biogeosciences 13, 1423–1437. doi:10.5194/bg-13-1423-2016.

Sagnotti, L., Scardia, G., Giaccio, B., Liddicoat, J.C., Nomade, S., Renne, P.R., Sprain, C.J., 2014. Extremely rapid directional change during Matuyama-Brunhes geomagnetic polarity reversal. Geophys. J. Int. 199, 1110-1124.

Shackelton, N.J., 1987. Oxygen isotopes, ice volume and sea level. Quaternary Science Reviews, 6, 183-190.

Sottili, G., Palladino, D.M., Zanon, V., 2004. Plinian activity during the early eruptive history of the Sabatini Volcanic District, Central Italy. Journal of Volcanology and Geothermal Research 135 (4), 361-379.

Sottili, G., Palladino, D.M., Marra, F., Jicha, B., Karner, D.B., Renne, P.R., 2010. Geochronology of the most recent activity in the Sabatini Volcanic District, Roman Province, central Italy. Journal of Volcanology and Geothermal Research 196, 20-30. doi:10.1016/j.jvolgeores.2010.07.003.

Steiger, R.H., Jäger, E., 1977. Subcommission on geochronology: convention on the use of decay constants in geo- and cosmochronology. Earth Planet. Sci. Lett. 6, 359-362.

Tzedakis, P.C., McManus J.F., Hooghiemstra, H., Oppo, D.W., Wumstra, T.A., 2003. Comparison of changes in vegetation in northeast Greece with records of climate variability in orbital and suborbital frequencies over the last 450 000 years. Earth and Planetary Science Letters, 212, 197-212

Tzedakis, P. C., Raynaud, D., McManus, J. F., Berger, A., Brovkin, V., et. al. 2009. Interglacial diversity. In: Nature Geoscience,2, (11), 751-755.

Tzedakis, P.C., Channell, J.E.T., Hodell, D.A., Kleiven, H.F., Skinner, L.C., 2012. Determining the natural length of the current interglacial. Nature Geoscience 5, 138–141.

Vakhrameeva, P., Koutsodendris, A., Wulf, S., Fletcher, W.J., Appelt, O., Knipping, M., Gertisser, R., Trieloff, M., Pross, J., 2018. The cryptotephra record of the Marine Isotope Stage 12 to 10 interval (460–335 ka) at Tenaghi Philippon, Greece: Exploring chronological markers for the Middle Pleistocene of the Mediterranean region. Quaternary Science Reviews 200, 313-333.

Villa, P., Soriano, S., Grün, R., Marra, F., Nomade, S., Pereira, A., Boschian, G., Pollarolo, L., Fang, F., Bahain, J.J., 2016a. The Acheulian and early Middle Paleolithic in Central Italy: Stability and Innovation. PLoS ONE 11(8) : e0160516. doi:10.1371/journal.pone.0160516.

Wagner, B., Wilke, T., Francke, A., Albrecht, C., Baumgarten, H., Bertini, A., Combourieu-Nebout, N., Cvetkoska, A., D'Addabbo, M., Donders, T.H., Föller, K., Giaccio, B., Grazhdani, A., Hauffe, T., Holtvoeth, J., Joannin, S., Jovanovska, E., Just, J., Kouli, K., Koutsodendris, A., Krastel, S., Lacey, J.H., Leicher, N., Leng, M.J., Levkov, Z., Lindhorst, K., Masi, A., Mercuri, A.M., Nomade, S., Nowaczyk, N., Panagiotopoulos, K., Peyron, O., Reed, J.M., Regattieri, E., Sadori, L., Sagnotti, L., Stelbrink, B., Sulpizio, R., Tofilovska, S., Torri, P., Vogel, H., Wagner, T., Wagner-Cremer, F., Wolff, G.A., Wonik, T., Zanchetta, G., Zhang, X.S., 2017. The environmental and evolutionary history of Lake Ohrid (FYROM / Albania): interim results from the SCOPSCO deep drilling project 2033–2054. doi:10.5194/bg-14-2033-2017

Wagner, B., Vogel, H., Francke, A., Friedrich, T., Donders, T., Lacey, J.H., Leng, M.J., Regattieri, E., Sadori, L., Wilke, T., Zanchetta, G., Albrecht, C., Bertini, A., Combourieu-Nebout, N., Cvetkoska, A., Giaccio, B., Grazhdani, A., Hauffe, T., Holtvoeth, J., Joannin, S., Jovanovska, E., Just, J., Kouli, K., Kousis, I., Koutsodendris, A., Krastel, S., Lagos, M., Leicher, N., Levkov, Z., Lindhorst, K., Masi, A., Melles, M., Mercuri, A.M., Nomade, S., Nowaczyk, N., Panagiotopoulos, K., Peyron, O., Reed, J.M., Sagnotti, L., Sinopoli, G., Stelbrink, B., Sulpizio, R., Timmermann, A., Tofilovska, S., Torri, P., Wagner-Cremer, F., Wonik, T., Zhang, X., 2019. Mediterranean winter rainfall in phase with African monsoons during the past 1.36 million years. Nature 573, 256-260.

Wulf, S., Keller, J., Paterne, M., Mingram, J., Lauterbach, S., Opitz, S., Sottili, G., Giaccio, B., Albert, P.G., Satow, C., Tomlinson, E.L., Viccaro, M., Brauer, A., 2012. The 100-133 ka record of Italian explosive volcanism and revised tephrochronology of Lago Grande di Monticchio. Quat. Sci. Rev. 58, 104-123.

Wulf, S., Keller, J., Satow, C., Gertisser, R., Kraml, M., Grant, K.M., Appelt, O., Vakhrameeva, P., Koutsodendris, A., Hardiman, M., Schulz, H., Pross, J. 2020. Advancing Santorini's tephrostratigraphy: New glass geochemical data and improved marine-terrestrial tephra correlations for the past ~360 kyrs. Earth-Science Reviews 200, 102964.

Zanchetta, G., Supizio, R., Roberts, N., Cioni, R., Eastwood, W.J., Siani, G., Caron, B., Paterne, M., Santacroce, R., 2011. Tephrostratigraphy, chronology and climatic events of the Mediterranean basin during the Holocene: an overview. The Holocene 21, 33–52.